HHS Public Access

Author manuscript

J Comp Neurol. Author manuscript; available in PMC 2024 January 01.

Published in final edited form as:

J Comp Neurol. 2023 January ; 531(1): 149–169. doi:10.1002/cne.25420.

Cellular distribution of the Fragile X mental retardation protein in the inner ear: a developmental and comparative study in the mouse, rat, gerbil, and chicken

Xiaoyu Wang[1,2], **Qiwei Fan**[1], **Xiaoyan Yu**[2], **Yuan Wang**[2]

[1]Division of Histology & Embryology, Key Laboratory for Regenerative Medicine of the Ministry of Education, College of Medicine, Jinan University, Guangzhou 510632, China

[2]Program in Neuroscience, Department of Biomedical Sciences, College of Medicine, Florida State University, Tallahassee, FL 32306, USA

Abstract

The Fragile X mental retardation protein (FMRP) is an mRNA binding protein that is essential for neural circuit assembly and synaptic plasticity. Loss of functional FMRP leads to Fragile X syndrome (FXS), a neurodevelopmental disorder characterized with sensory dysfunction including abnormal auditory processing. While the central mechanisms of FMRP regulation have been studied in the brain, whether FMRP is expressed in the auditory periphery and how it develops and functions remains unknown. In this study, we characterized the spatiotemporal distribution pattern of FMRP immunoreactivity in the inner ear of mice, rats, gerbils, and chickens. Across species, FMRP was expressed in hair cells and supporting cells, with a particularly high level in the immature hair cells during the prehearing period. Interestingly, the distribution of cytoplasmic FMRP displayed an age-dependent translocation in hair cells, and this feature was conserved across species. In the auditory ganglion (AG), FMRP immunoreactivity was detected in neuronal cell bodies as well as their peripheral and central processes. Distinct from hair cells, FMRP intensity in AG neurons was high both during development and after maturation. Additionally, FMRP was evident in mature glial cells surrounding AG neurons. Together, these observations demonstrate distinct developmental trajectories across cell types in the auditory periphery. Given the importance of peripheral inputs to maturation of auditory circuits, these findings implicate an involvement of FMRP in inner ear development as well as a potential contribution of periphery FMRP to the generation of auditory dysfunction in FXS.

Graphical Abstract

Corresponding authors: Yuan Wang, Ph.D., 1115 West Call Street, Florida State University, Tallahassee, FL 32306, USA, Phone: (850) 645-4934; yuan.wang@med.fsu.edu, Xiaoyu Wang, Ph.D., 601 West Huangpu Avenue, Tianhe District, Guangzhou 510632, China, Phone: (020) 85220254; wangxiaoyu@jnu.edu.cn.

Conflict of Interest

The authors declare no conflict of interests.

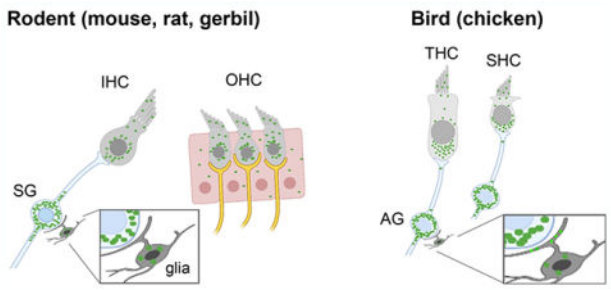

The Fragile X mental retardation protein (FMRP) is an mRNA binding protein, loss of which leads to Fragile X syndrome, a neurodevelopmental disorder characterized with abnormal auditory processing. This study provides the first description of FMRP distribution pattern in the developing and mature auditory inner ear of rodents and birds.

Keywords

Fragile X syndrome; cochlea; auditory processing; spiral ganglion; hair cell; sensory periphery; brain development

INTRODUCTION

Fragile X syndrome (FXS) is a leading cause of inherited forms of intellectual disability, which in most cases is the result of the loss of Fragile X mental retardation protein (FMRP) (Verkerk et al., 1991; Verheij et al., 1993; Penagarikano et al., 2007; Bagni et al., 2012; Santoro et al., 2012). FMRP, encoded by the *FMR1* gene, is an mRNA binding protein that is broadly expressed across cell types (neurons, astrocytes, and microglia) in healthy brains (Pacey and Doering, 2007; Gholizadeh et al., 2015; Zorio et al., 2017). A major known function of FMRP is to regulate local protein translation of associated mRNAs at specialized neuronal sites including dendrites, axons, and synapses (Davis and Broadie, 2017). Animals without FMRP have exhibited abnormal neuronal differentiation, altered dendritic arborization, axonal misprojection, and compromised synaptic plasticity (Huber et al., 2002; Deng et al., 2011, 2013; Pacey et al., 2013; Wang et al., 2018, 2020). Individuals with FXS display autism-like behaviors, poor language development, and prominent sensory abnormalities (Hagerman et al., 2017; Rais et al., 2018). In the auditory system, FXS patients exhibit hypersensitivity to auditory stimuli, impaired habituation to repeat sounds, reduced auditory attention, and difficulties in complex hearing, phenotypes that may also be associated with problems in social interactions and language development (Rotschafer and Razak, 2014; Sinclair et al., 2017; Rais et al., 2018).

It is not clear how these auditory-related phenotypes emerge in the absence of FMRP. In the brain, FMRP is normally expressed at high levels in auditory neurons at both cortical and subcortical levels (Beebe et al., 2014; Wang et al., 2014; Zorio et al., 2017; Yu et al., 2021). Studies of animal models of FXS (*Fmr1* knockout) have identified a wide range of molecular, morphological, and physiological abnormalities in the auditory central nerve system (CNS) from the brainstem and midbrain to the cortex (Constantin et al., 2020; McCullagh et al., 2020). Intriguingly, there is evidence of changes at the entry of acoustic

signals to the brain, showing reduced and/or delayed auditory responses at the level of the auditory nerve (Arinami et al., 1988; Ferri, 1989; Kim et al., 2013; Rotschafer et al., 2015; El-Hassar et al., 2019), suggesting abnormal development of the auditory periphery and auditory nerve when FMRP is absent. It is well appreciated that proper development of the auditory CNS critically depends on afferent inputs (spontaneous or sensory-driven) from the cochlea through the auditory nerve (Rubel and Fritzsch, 2002; Ryugo, 2015; Connelly et al., 2017). Thus, it is possible that peripheral expression of FMRP is required for normal development of the cochlea and that loss of cochlear FMRP contributes to the generation of the central auditory dysfunction seen in FXS. Interestingly, among human FXS patients who had no evidence of a periphery hearing problem (conductive and sensorineural hearing loss), auditory brainstem function appears normal (Roberts et al., 2005), further supporting the presence of a peripheral mechanism underlying the auditory phenotypes in FXS. However, whether and how FMRP is expressed in the auditory organ of the inner ear (i.e., the cochlea) has not been investigated.

In this study, we aimed to determine the developmental profile of FMRP expression and localization in the cochlea using immunocytochemistry, with an emphasis on hair cells and auditory ganglion (AG) neurons (also called spiral ganglion neurons or SG neurons in mammals) that give rise to the auditory nerve. Hair cells in the mammalian cochlea are auditory receptors that transform mechanical vibrations into electrical signals. They are situated in the organ of Corti and surrounded by supporting cells. Upon acoustic stimulation, hair cells release neurotransmitters to trigger action potentials in the AG/SG neurons, which in turn send the signal to the brainstem via their central axons in the auditory nerve. We characterized FMRP distribution in the cochlea and compared it across three rodent species (mouse, rat, gerbil) and an avian species (chicken), all popular animal models for understanding auditory development, function, and pathology. While mice and rats are high-frequency listeners, gerbils and chickens are sensitive to low-frequency sounds (Ryan, 1976; Kelly and Masterton, 1977; Heffner et al., 2001; Hill et al., 2014); thus, the four models cover the hearing range of humans. In the chicken inner ear, hair cells are situated in the basilar papilla (BP) in the auditory duct and innervated by AG neurons, comparable to the mammalian system. For each species, we examined FMRP distribution at both developing and mature stages, with the goal of identifying both fundamental features of FMRP distribution in the auditory periphery as well as its cell type-specific variations and age-dependent dynamics.

MATERIALS AND METHODS

Animals

Breeders for *Fmr1* knockout (KO) mice (Hemi FVB. 129P2-Pde6b+; #004624) and their wildtype (WT) littermates (FVB. 129P2-Pde6b+; #004828) were purchased from the Jackson Laboratory (Bar Harbor, ME) and used to set up colonies in a Florida State University (FSU) vivarium. Mouse pups were used between the ages of postnatal (P) day 6 (P6) and 6 months. Likewise, breeders for Mongolian gerbils (*Meriones unguiculatus*), strain 243, were purchased from the Charles River Laboratories (Wilmington, MA) and used to set up a gerbil colony in a FSU vivarium. Gerbil pups were used between the ages of P6 and

P56. Wistar rats (*Rattus norvegicus*) were a gift from Dr. Dongqing Cai at Jinan University. Rat pups were used at ages P2, P6, P14, and 6 months. Fertilized chicken eggs were obtained from the Charles River Laboratories and incubated in an FSU vivarium. Chicken embryos between embryonic (E) day 2 and 20 (E2–20) were used. For each species, animals of both sexes were used. All procedures were approved by the FSU and Jinan University Institutional Animal Care and Use Committees and conformed to National Institutes of Health guidelines.

Immunocytochemistry

The rodents were anesthetized with a mixture of ketamine and xylazine and transcardially perfused with 0.9% saline followed by 4% paraformaldehyde in 0.1M phosphate buffer. The temporal bones were removed from the skull and postfixed overnight in the same fixative before the cochleae were dissected out. For chicken embryos, the BP was dissected out after overnight fixation of the skull. The cochleae and BPs were then transferred to 30% sucrose in phosphate buffer until they settled. After being embedded in a medium containing 10% gelatin and 20% sucrose, the cochleae were cross-sectioned at 20 μm using a cryostat. Sections were mounted on gelatin-coated slides for immunohistochemistry.

For immunostaining, slides were washed with 0.01M phosphate buffered saline (PBS) at 37°C for 5 minutes to remove the gelatin, followed by three additional 10-minute washes in PBS at room temperature. Slides were incubated with primary antibody solutions diluted in PBS with 0.3% Triton X-100 overnight at 4°C. Table 1 lists the antigens, concentrations, and RRID citations of the primary antibodies used in this study. The optimal antibody concentration was determined through a series of concentration tests to avoid floor or ceiling truncation. Following primary antibody incubation, slides were treated with Alexa-Fluor secondary antibodies (Life Technologies, Carlsbad, CA) at 1:500 for 4 hours at room temperature. Some sections were counterstained with DAPI at 1:1000 and incubated with secondary antibodies. Slides were washed and coverslipped with Fluoromount-G mounting medium (SouthernBiotech, Birmingham, AL).

Western blot

Protein samples were harvested from flash frozen WT or *Fmr1* KO mouse cochleae at P7 and chicken BPs at E9, E11, E15, and E19. For each age, genotype, and species, 3–5 animals were used and each animal was considered as an individual data point. Samples were homogenized in EDTA buffer (62.5 mM Tris-HCl pH 6.8, 2% SDS, 10% glycerol, 5% β-ME, 10 mM EDTA) using the Ultra-Turrax T10 homogenizer (IKA Works, Inc., Wilmington, NC). Equal amounts of protein lysates in loading buffer (2% SDS, 125 mM Tris-HCl pH 6.8, 10% glycerol, 0.025% bromophenol blue, and 5% 2-mercaptothanol) was denatured at 95°C for 5 min, resolved in NuPAGE 4–12% Bis-Tris Gels (Life Technologies, Carlsbad, CA), and then transferred onto PDVF membranes (GE Healthcare, Chicago, IL). After blocking in 5% milk in Tris-buffered saline with 0.1% Tween-20 (TBST) for 1h at room temperature, membranes were probed against the primary antibodies diluted in TBST overnight at 4°C in 1% milk in TBST. Membranes were then incubated with either HRP or fluorescent secondary antibodies for 1h at room temperature. HRP-conjugated secondary antibodies were used at 1:5000 (Santa Cruz Biotechnology, Inc., Dallas, TX)

and blots were developed with SuperSignal West Pico Chemiluminescent Substrate (Thermo Fisher Scientific) and exposed to X-ray film. Fluorescent IRDye 800CW goat anti-rabbit and IRDye 680RD goat anti-mouse secondary antibodies were used at 1:20,000 (LI-COR Bioscience, Lincoln, NE). Blots were scanned with an Odyssey-CLx Infrared Imaging system (LI-COR Bioscience). Glyceraldehyde-3-phosphate dehydrogenase (GAPDH), and β-tubulin were used as loading controls.

In ovo electroporation

An *Fmr1* shRNA (gaggatcaagatgcagtgaaata; nucleotides 951–973 of chicken *Fmr1*) was synthesized and cloned into a transposon-based vector system with a Tol2 vector containing doxycycline regulatory components and an EGFP reporter as previously described (Wang et al., 2018). For hair cell and AG neuron transfection, *in ovo* electroporation was performed, following the procedure as described in Fan et al. (2022), at stage HH13 (Hamburger and Hamilton, 1951) by injecting the plasmids into the right otocyst, which contains hair cell precursors and delaminating neuroblasts (summarized by Chervenak et al., 2013). A platinum bipolar electrode was placed to the anterior and posterior sides of the otocyst, delivering short electrical pulses (4 pulses at 20 volts with 30 ms duration and 10 ms between pulses). Following electroporation, the eggs were returned to the incubator. At E8, 50 μl of 1 mg/ml doxycycline (Sigma Cat#. D9891) was added onto the chorioallantoic membrane to trigger the transcription of shRNA. The administration was performed again every other day to maintain the expression before BP dissection at desired developmental stages.

For genetic labeling of satellite glial cells in the chicken AG, EGFP was cloned into a transposon-based vector system as previously described (Wang et al., 2020). *In ovo* electroporation was performed at E2 by injecting the plasmids into the neural tube where the satellite glial cell precursors were located (Jessen and Mirsky, 2005). A platinum bipolar electrode was placed on the two sides of the neural tube, delivering short electrical pulses (4 pulses at 20 volts with 30 ms duration and 10 ms between pulses). Following electroporation, the eggs were returned to the incubator until the desired stage for dissection.

Quantification of FMRP intensity

The intensity of FMRP immunoreactivity in hair cells and ganglion neurons was quantified and compared across developmental stages in mice, rats, and chickens. Image stacks were collected with a 63X oil-immersion lens at a resolution of 11 pixels per micron at XY dimensions and with a Z interval of 2 μm using a Leica SP8 confocal microscope. All images from the same animal were captured with the same imaging parameters. For each cell/neuron, the measurement was performed on the focal plane with maximum somatic area and an identifiable DAPI-stained nucleus. FMRP intensity was measured as the mean gray value of FMRP staining intensity following background subtraction using Fiji software (National Institutes of Health, USA). For mice, the ratio of FMRP intensity between hair cells and supporting cells was also calculated by normalizing FMRP intensity in each hair cell to the mean of FMRP intensity across all measured supporting cells on the same sections. For statistical analyses, the FMRP intensities were grouped from all cells and animals of the same age. One-way ANOVA followed by Tukey’s multiple comparison was

performed for each species across age groups using Prism software (GraphPad Software, La Jolla, CA). All data are presented as mean ± standard deviation (SD) in the figures, and $p < 0.5$ was considered statistically significant.

Imaging for illustration

Images for illustration were captured with an Olympus FV1000 or a Leica SP8 confocal microscope. Image brightness, gamma, and contrast adjustments were performed in Adobe Photoshop (Adobe Systems, Mountain View, CA). All adjustments were applied equally to all images of the same set of staining from the same animal unless stated otherwise.

RESULTS

FMRP detection in the mouse cochlea

The specificity of FMRP antibodies has not been validated in the vertebrate ear. Here, we characterized three commercially available antibodies using P6–7 mouse cochlea samples. These include a monoclonal antibody, CST7104, and two polyclonal antibodies, Ab17722 and PA5; all three were generated against the C-terminus of human FMRP (Table 1). Western blot for CST7104 exhibited a single band on WT samples (Figure 1a). This band was absent on *Fmr1* KO mice, demonstrating a high specificity for CST7104 in recognizing cochlear FMRP. Immunocytochemistry revealed CST7104 immunoreactivity in the WT mouse cochlea, with a particularly robust staining in the spiral ganglion (SG) (Figure 1b). In contrast, *Fmr1* KO mice showed no detectable immunoreactivity in the hair cells or SG, except for a nonspecific staining along the edge of the modiolus (arrows in Figure 1c).

Similar to CST7104, Ab17722 and PA5 recognized specific western blot band(s) on WT but not *Fmr1* KO samples (Figure 1d, 1g). Both Ab17722 and PA5 displayed additional, weaker bands in both WT and *Fmr1* KO (star in Figure 1d and 1g). On cochlea cross-sections, Ab17722 and PA5 exhibited a comparable pattern of immunostaining as CST7104, with two differences. First, Ab17722 showed a strong labeling of the tectorial membrane (TM) in the WT but not the *Fmr1* KO, indicating an FMRP association (Figure 1e–f). This labeling was less dramatic for PA5 (Figure 1h–i) and was not observed for CST7104. Second, a small population of SG neurons were Ab17722- or PA5-immunoreactive in the *Fmr1* KO cochlea (Figure 1f,1i), which was not seen in CST7104-stained sections. This nonspecific staining is more prevalent for PA5 as compared to Ab17722.

Based on these overall staining patterns, we concluded that among the three antibodies, monoclonal CST7104 is the more specific antibody for examining FMRP distribution *in situ* in the rodent cochlea using immunocytochemistry. Polyclonal Ab17722 and PA5 detected more FMRP-specific labeling than CST7104 (such as in TM) while introducing some degree of nonspecific staining (such as in SG). To characterize FMRP expression and subcellular localization in the cochlea, we used both CST7104 and Ab17722 for FMRP identification and performed age-matched *Fmr1* KO control for each identification.

FMRP in the developing and mature mouse cochlea: organ of Corti

In mice, hearing onset takes place around P12–14. We examined FMRP expression pattern using CST7104 at a prehearing age (P7), shortly after hearing onset (P14), and at an adult age of 3 months. In the organ of Corti, the overall intensity of CST7104 immunostaining was high at P7 and gradually declined at P14 and 3 months (Figure 2a1–c1). At P7, FMRP exhibited a diffused distribution in the cytoplasm of inner hair cell (IHC), outer hair cells (OHC), and supporting cells (Figure 2a2). The staining was notably stronger in hair cells than in supporting cells. In hair cells, cytoplasmic FMRP immunoreactivity appeared stronger around the nucleus, particularly in the apical portion (Figure 2a3). This subcellular pattern was also seen at P14, but less distinct, accompanied by an overall reduction in immunostaining intensity (Figure 2b2–b3). Additionally, we observed a nucleus translocation of IHCs from the bottom to a more centered place in the cytoplasm, which was not seen in OHCs (Figure 2b2–b3). By 3 months, FMRP immunostaining was faint in both hair cells and supporting cells (Figure 2c2–c3). Quantitatively, we identified a decrease in the mean FMRP intensity from P14 to 3 months for both IHCs (Figure 2d) and OHCs (Figure 2e). Additionally, we normalized FMRP intensity in individual hair cells to the average FMRP intensity of supporting cells measured from the same sections, given the consistently low levels of FMRP in the supporting cells across ages. There was no significant difference in FMRP intensity in OHCs relative to supporting cells (Figure 2g), indicating a comparable trajectory and similar degrees of age-dependent FMRP downregulation between the two cell types. In contrast, FMRP intensity in IHCs relative to supporting cells was increased at P14 and 3 months as compared to P6 (Figure 2f). This indicates higher relative FMRP levels, and thus lower degrees of FMRP downregulation across ages, in IHCs compared with OHCs or supporting cells.

We further examined P6 (a prehearing age) and P56 (a mature age) mouse cochleae using Ab17722 (Figure 3). This antibody demonstrated a developmental profile of FMRP similar to that observed in CST7104 immunostaining. FMRP intensity in hair cell (IHC and OHC grouped together) was significantly reduced from P6 to P56 (Figure 3d). Two additional features, however, were detected by Ab17722. First, Ab17722 revealed FMRP immunoreactivity in phalloidin-labeled hair bundles of IHCs and OHCs at P6 in the WT but not *Fmr1* KO mouse (insets in Figure 3a1). Second, an intense staining appeared just below the cell body of OHCs, but not IHCs, at P56 (blue arrowheads in Figure 3b2). This staining was dramatically weaker, although detectable, in age-matched *Fmr1* KO mice (Figure 3c2). These observations identified additional FMRP localization in hair cell bundles of immature hair cells and possibly in some structures around hair cells in the mature mouse organ of Corti.

FMRP in the developing and mature mouse cochlea: spiral ganglion (SG)

Mouse SG showed high levels of FMRP immunoreactivity as detected by CST7104 during development. Strong immunoreactivity was present in the majority, if not all, neuronal cell bodies at P7, P14, and 3 months in WT (Figure 4a–b, d–i) but not *Fmr1* KO (Figure 4c) mice. Because there was no clear regional variation across the apical-basal length of the SG at any given age, we quantified FMRP intensity across all SG neurons measured from animals of the same age. The FMRP intensity per SG neuron increased along with age

(Figure 4j). Beyond the cell body, FMRP immunoreactivity was present in the processes of SG neurons (Figure 4k). SG neurons have a periphery process that innervates hair cells, and a central axon that projects to the cochlear nucleus in the brainstem; both can be visualized by immunostaining of Tuj1, the neuron-specific class III beta-tubulin. Double labeling of FMRP and Tuj1 immunoreactivities revealed FMRP localization in the proximal portions of Tuj1-labeled peripheral and central axons.

Observations from Ab17722-stained sections demonstrated a comparable pattern of FMRP in the mouse SG. In WT, FMRP immunoreactivity was strong at P6 and appeared even stronger at P56 throughout the SG (Figure 5a–b, d–g). A small group of SG neurons exhibited a particularly intense staining (blue stars in Figure 5d), which may be associated with the nonspecific staining of Ab17722 in some SG neurons of *Fmr1* KO mice (arrowheads in Figure 5c). FMRP immunoreactivity in the processes of SG neurons was more prominent in AB17722 immunostaining than CST7104 (blue arrows in Figure 5e–f, 5h). Additional Ab17722 immunoreactivity was found between SG neuronal cell bodies, presumably glial cells and/or neuronal processes. This localization was not observed in *Fmr1* KO mice, indicating its specificity to FMRP.

FMRP in the developing and mature rat cochlea

We examined the cellular distribution of FMRP in the rat cochlea at P2, P6, P14 and 6 months using CST7104. Similar to mice, FMRP immunoreactivity was strong in the rat organ of Corti at P2–6 and declined afterward (Figure 6). At P2 and P6, the intense FMRP immunoreactivity, particularly in the region above the nucleus of IHCs and OHCs, readily differentiated hair cells from the surrounding supporting cells, which were moderately labeled (Figure 6a–f). At P14, FMRP intensity was notably reduced in the organ of Corti (Figure 6g–i), although a perinuclear staining pattern was still present in OHCs. By 6 months, FMRP immunoreactivity was weak in the organ of Corti (Figure 6j–l). Quantitative analyses confirmed a graduate decline of FMRP intensity in hair cells after P6 (Figure 6n). As in mice, the nucleus of the rat IHC showed a translocation from the bottom to the center of the cytoplasm with age, and FMRP distribution in the IHC was accumulated in the apical cytoplasm at young ages and then concentrated in the basal cytoplasm (Figure 6m). In contrast, the nucleus location and FMRP distribution in OHCs were stable between P6 and 6 months.

Examinations of the SG demonstrated a high level of FMRP immunoreactivity in the neuronal somata, with the highest intensity at 6 months (Figure 7a–h, k). Similar to mice, there were no notable differences across the apex to base dimension. Double labeling of FMRP and Tuj1 revealed FMRP localization in the proximal portions of Tuj1-labeled peripheral and central processes of SG neurons (Figure 7i–j). Triple labeling of FMRP, Tuj1, and DAPI further identified a FMRP localization in a group of small cells. These cells were Tuj1-negative and had a condensed nucleus (asterisks in Figure 7j).

FMRP in the developing and mature gerbil cochlea

We examined the cellular distribution of FMRP in P6 and P56 gerbil cochleae using Ab17722. At both ages, FMRP immunostaining was generally weak throughout the

midmodiolar section except for the SG (Figure 8a, d). At P6, hair cells were more darkly labeled than the other cell types in the organ of Corti and displayed a perinuclear distribution, which is similar to what was observed in mice and rats (Figure 8b). Later at P56, however, a perinuclear pattern was not evident in either IHCs or OHCs, showing a more uniform distribution in the cytoplasm (Figure 8e). On the other hand, strong FMRP immunoreactivity was seen throughout the SG (Figure 8c, f). FMRP immunostaining in SG neurons appeared weaker and more punctate at P56 as compared to P6. A small population of SG neurons had exceptionally intense staining, similar to the observations from mice, which were considered a nonspecific effect of the antibody Ab17722.

Characterization of a FMRP antibody in the chicken basilar papilla (BP)

We have previously developed a polyclonal antibody, PA8263, that recognizes chicken FMRP on brain samples (Yu et al., 2020). Here we validated the specificity of PA8263 on the chicken cochlea duct. Western blot on the cochlea duct collected from E9–E19 chicken embryos displayed one single band (Figure 9a), similar to what was observed on brain samples (Yu et al., 2021). Normalized FMRP band intensity to β-actin remained unchanged from E9 to E19 (Figure 9b). To further validate the antibody specificity, we transfected a subset of hair cells and supporting cells via *in ovo* electroporation of a chicken *Fmr1* shRNA-EGFP (Wang et al., 2018). PA8263 immunoreactivity was dramatically reduced in transfected cells (yellow solid circles; EGFP positive) as compared to neighboring non-transfected cells (white dashed circles; EGFP negative) (Figure 9c–d). Similarly, AG neurons exhibited strong PA8263 immunostaining in control, non-transfected (white dashed circles; EGFP negative) but not *Fmr1* shRNA-EGFP-transfected (yellow solid circles; EGFP positive) neurons (Figure 9e–f). These observations demonstrate a high specificity of PA8263 in recognizing chicken FMRP in the inner ear. All of the following FMRP immunodetection in chickens was therefore performed using this antibody.

FMRP in the developing chicken basilar papilla (BP)

The avian BP is the auditory sense organ that is the analogue to the mammalian organ of Corti. We examined FMRP distribution in the chicken BP at three developmental stages: E9 (before the hearing onset), E15 (around the hearing onset), and E19 (the age at which the auditory system is considered morphologically mature). At E9, FMRP immunostaining was intense in the BP and AG (Figure 10a). Hair cells showed higher levels of immunoreactivity than the supporting cells located below (Figure 10b). Notably, a number of darkly labeled FMRP-immunoreactive puncta were present within the supporting cell layer that was immediately adjacent to hair cells (blue arrows in Figure 10b). Different from the mammalian IHCs and OHCs, the avian hair cells have two types: tall hair cells (THCs), located on the attached part of the basilar membrane; and short hair cells (SHCs), located on the free basilar membrane (Tanaka and Smith, 1978). At E9, THCs and SHCs are differentiable based on their cell body shape, with THCs being lenticular and SHCs more columnar. Both hair cell types exhibited a uniform distribution of FMRP immunoreactivity in the cytoplasm (Figure 10c). At E15, the overall signal intensity was reduced in the BP (Figure 10d). FMRP immunoreactivity in both THCs and SHCs was reduced as compared to E9 (Figure 10e). Interestingly, FMRP immunoreactivity in both THCs and SHCs accumulated around the nucleus, particularly in the basal region (arrows in

Figure 10f). Substantial FMRP immunoreactivity was also identified in the apical region of THCs but not of SHCs. At E19, hair cells became more distinct because of their high levels of FMRP immunostaining relative to the supporting cells (Figure 10g–h). In both THCs and SHCs, FMRP was concentrated in the basal region (arrows in Figure 10i). Quantitative analyses confirmed a decline of FMRP intensity in hair cells with age from E9 to E19 (Figure 11a). Taken together, the intensity and subcellular localization of FMRP are highly dynamic in chicken hair cells during development.

We next determined whether FMRP is located in the hair bundles. We visualized hair bundles via both bright field imaging with phase contrast (Figure 12a) and genetic labeling following *in ovo* electroporation of *Fmr1* shRNA-EGFP (Figure 12b). FMRP immunoreactivity was detected in the hair bundles of control, non-transfected hair cells (asterisk in Figure 12a–d; white dashed circle in Figure 12e; EGFP negative) but not in the hair bundles of neighboring *Fmr1* shRNA-EGFP-transfected hair cells (yellow solid circle in Figure 12e; EGFP positive). In most hair cells, FMRP signal appeared only along the long cilium within the hair bundle.

FMRP in the developing chicken auditory ganglion (AG)

In the chicken AG (analogue to the mammalian SG), FMRP immunostaining was consistently strong during development. AG neurons displayed robust FMRP immunostaining as early as E6, standing out against the surrounding head mesenchyme (Figure 13a). Closer observations demonstrate a punctate pattern of FMRP in the cytoplasm of AG neurons (Figure 13b). A weak but detectable localization was also seen in the nucleus of AG neurons. The staining pattern of FMRP maintained at E9, E15, and E19 (Figure 13c–h). Quantitative analyses revealed an increase in somatic FMRP intensity in AG neurons with age during this developmental period (Figure 11b).

Starting at E15, additional FMRP immunoreactivity was detected among neuronal cell bodies. By E19, AG neurons were often enveloped by a layer of FMRP-immunoreactive structures (arrows in Figure 14h), a feature that was not present at earlier stages. To determine the nature of these signals, we counterstained the cochlea sections with DAPI along with double immunostaining of FMRP and Tuj1, a neuronal marker. We identified the cells with a condensed DAPI staining but Tuj1-negative as non-neuronal glial cells. Such cells were rare at E9 (Figure 14a–c), but consistently present at E15 and E19 (asterisks in Figure 14d–i). No FMRP immunoreactivity was found around or within the DAPI-stained nucleus of the glial cells at E15. At E19, however, FMRP immunoreactivity was frequently identified in the glial cytoplasm. FMRP-immunoreactive envelopes surrounding the Tuj1-expressing AG neurons were Tuj1-negative and could be traced back to the FMRP-immunoreactive glial cell bodies (arrows in Fig. 14g–i). Together, these observations identified FMRP expression in the satellite glial cells in the developed (E19) but not immature (E15) chicken AG.

To further confirm the lack of FMRP expression in satellite glial cells at E15, we employed a selective genetic labeling method for a better visualization of these cells. Peripheral glial cells are derived from the neural crest from a group of cells located on the dorsal neural tube (Jessen and Mirsky, 2005). Therefore, we performed *in ovo* electroporation to introduce

EGFP-expressing plasmids into the neural crest progenitors and visualized EGFP-positive cells in the AG at E15 (Figure 14j). These glial cells were small in size and located among the large neuronal cell bodies (asterisks in Figure 14k). FMRP immunoreactivity in these glial cells was barely detectable or just slightly above the background level, in high contrast to strongly labeled AG neurons (Figure 14l).

Finally, we determined FMRP localization in the axonal processes of AG neurons using either neurofilament (NF) or Tuj1 as an axonal marker. At E9, the peripheral processes of AG neurons have reached to the hair cells (Figure 15a), passing the supporting cell layer where distinct FMRP-immunoreactive puncta were found (Figure 15b–c). High-magnification images confirmed a localization of FMRP puncta on NF-labeled processes of AG neurons (Figure 15d). This localization persisted at E15 (Figure 15e–h) and E19 (Figure 15i–l). However, the size of the FMRP-immunoreactive puncta was reduced at these later ages as compared to E9 (Figure 15m).

DISCUSSION

This study provides the first description of FMRP distribution pattern in the auditory inner ear (i.e., the cochlea) across species and over developmental stages. Important observations are summarized in Figure 16, including: (1) FMRP is expressed in hair cells during the prehearing period and then downregulated during maturation. (2) FMRP is localized in the cell bodies and stereociliary bundles of hair cells. (3) FMRP expression in AG neurons is strong during prehearing and further upregulated with age. (4) FMRP is localized in the cell bodies as well as the distal and/or basal processes of AG neurons. (5) No tonotopic variation in cellular FMRP intensity was detected for either hair cells or AG neurons. (6) The above developmental features (1–5) are conserved across avian and rodent species regardless of their hearing ranges, although interspecies variations exist on specific patterns. (7) Glial expression of FMRP is evident in the mature rat SG and in the avian AG after hearing onset. Here we discuss the significance of these observations in relation to the postnatal development and mature functions of the inner ear, followed by implications in understanding the emergence of auditory deficits in FXS.

Antibody detection of periphery FMRP

We validated the specificity of the primary antibodies with both western blot and immunocytochemistry, and importantly, with appropriate negative controls using KO and knockdown methods. It is known that the mouse FMRP has at least 12 isoforms in the brain (Brackett et al., 2013), which may appear as multiple bands on western blot. The current study identified a single band for the monoclonal antibody CST7104 and multiple FMRP-specific bands for the polyclonal antibodies Ab17722 and PA5 (Figure 1). This may imply that Ab17722 and PA5 identify more FMRP isoforms than CST7104, although this requires further investigation. Thus, combining observations from multiple antibodies (for the case of mice) is also important to both achieve the specificity and enhance the completeness of identification. For example, FMRP localization in the mouse hair bundle was observed by using Ab17722 but not CST7104. However, this localization was convincingly confirmed in chickens in which within-animal validations between neighboring hair bundles with and

without *Fmr1* expression were possible (see Figure 12). On the other hand, using Ab17722 alone would not lead to conclusive results regarding FMRP distribution in the SG, as a small neuronal population were immunoreactive to this antibody in *Fmr1* KO mice.

The two antibodies used to detect rodent FMRP (CST7104 and Ab17722) target a c-terminal portion of the full-length protein that is preserved across the exon 14-containing isoforms of the mammalian FMRP (Eichler et al., 1993; Brackett et al., 2013). Isoforms lacking exon 14 have a c-terminal different from the full-length isoform of FMRP due to frame shifts (Dury et al., 2013). In Hela cells, these isoforms have the ability to enter the nucleus and localize to Cajal bodies (Dury et al., 2013). If these isoforms are expressed in the mammalian cochlea, they were not detected in this study. Similarly, the PA8263 for recognizing chicken FMRP would fail to detect the isoforms with c-terminal frame shifting, if such isoforms exist.

Cellular distribution of FMRP in developing hair cells

FMRP is expressed in hair cells, with a conserved developmental trajectory between rodents and birds. The cytoplasmic intensity of FMRP is high at prehearing ages (mice and rat: P2–7; chicken: E9–15) and significantly reduced afterward. This pattern resembles what was observed in the brain, where FMRP levels decline rapidly around postnatal weeks 2–3 in rodents (Lu et al., 2004; Wang et al., 2004; Cook et al., 2011; Pacey et al., 2013). In both the mouse and chicken, the age-dependent FMRP decline occurs across hair cell types. Further analyses in mice, however, demonstrated different profiles of this process between IHCs and OHCs. FMRP intensity in OHCs appears to decline at a similar rate with the surrounding supporting cells, maintaining a OHC/supporting cell ratio of 1.4–1.6 from P7 to 3 months (see Figure 2g). In contrast, FMRP intensity in IHCs reduces slower so that FMRP intensity in IHCs is about 1.6 and 2.6 times higher than that in supporting cells at P6 and P14, respectively. As a consequence, FMRP level is comparable between IHCs and OHCs during early development (P7) and is significantly higher in IHCs than in OHCs and supporting cells at older ages (P14 and 3 months).

Observations of FMRP distribution in the hair cell cytoplasm at the subcellular level revealed a general theme across species as well as interspecies variations between rodents and birds. Across species, FMRP displays a concentrated distribution in areas around the nucleus, and this pattern is more obvious in developing systems, before and around the onset of hearing, than after maturation (heatmaps in Figures 2, 3, 6, and 10). Additionally, the mouse and rat IHCs exhibit a shift of FMRP distribution from the luminal portion of the cytoplasm at early ages (P6–7) to the basal portion, where ribbon synapses are situated, at older ages. This transition is not found in OHCs, in which FMRP is primarily located in the luminal portion of the cell body, the site for motility, across ages. No subcellular shifting was found in chickens, in which FMRP is relatively uniform between the luminal and basal cytoplasm and then becomes more concentrated in the basal portion of cell bodies later for both THCs and SHCs. The avian THCs and SHCs are comparable to the mammalian IHCs and OHCs, respectively, with regard to their afferent and efferent innervation patterns (Fischer, 1994). Unlike the mammalian OHCs, the avian SHCs are not mobile. Whether the two variations across hair cell types, FMRP localization and cell body mobility, are associated is unknown.

The shift of FMRP distribution in hair cells is the accompanied with the upward nucleus translocation in the rodent IHCs, which is less obvious for OHCs and avian hair cells. As far to our knowledge, this age-dependent nucleus repositioning has not been reported previously. The significance of this developmental event is unknown; however, abnormal nucleus location in cell bodies has been reported to cause progressive high-frequency hearing loss (Horn et al., 2013).

One intriguing finding of this study is the identification of FMRP localization in the hair bundles, which was found in both the mouse (see Figure 3) and chicken (see Figure 12). This localization is most dramatic in the tallest portion of the hair bundles in chickens, presumably the kinocilium, while it appears more diffuse in the mouse hair bundles. Further investigations with high-resolution TEM imaging should be conducted to clarify the exact location of FMRP in the hair cell bundles. Pcdh15, a key component of the tip link situated at the tip of the shorter stereocilia (Kazmierczak et al., 2007; Sotomayor et al., 2012; Zheng and Holt, 2021), may be a potential target for FMRP, given the known association of FMRP with mRNAs of several protocadherin (Pcdh) family members (Darnell et al., 2011). Mechanically-gated potassium channels at the tip of hair bundles present another likely mechanism for FMRP regulation. In the brain, FMRP deficiency alters the expression and conductance of potassium channels (Brown et al., 2010; Ferron, 2016; El-Hassar et al., 2019; Zhan et al., 2020).

FMRP distribution in the auditory ganglion (AG) and spiral ganglion (SG)

We identified a strong FMRP expression in neurons throughout the AG of birds and SG of rodents. Unexpectedly, FMRP expression in the AG is strong at all ages examined and further enhances with maturation. This is distinct from the developmental trajectory of FMRP expression in the organ of Corti (this study) or in the brain (Lu et al., 2004; Wang et al., 2004; Cook et al., 2011; Pacey et al., 2013), in which FMRP expression peaks during development and declines with age. This unique feature strongly implicates the importance of FMRP to both the development and mature functions of the AG. Indeed, AG neurons are a highly specialized cell type with a bipolar axonal configuration, innervating both hair cells and the brainstem. We have identified FMRP localization in the proximal portion of the periphery and central processes in mice and rats (see Figures 5, 7), though this is less clear in gerbils and chickens. In chickens, distinct FMRP puncta were present in the distal portion of the periphery processes before the terminals (see Figure 15), which was not seen in rodents. Instead, a strong localization of FMRP immediately adjacent to the cell body of the mouse OHCs resembles the location of presynaptic terminals. Together, these observations demonstrate that FMRP can localize in the distal and possibly terminal portion of the AG projection on hair cells with interspecies variations. This localization is consistent with FMRP as a component of RNA granules in neuronal extensions for distal protein translation (Lai et al., 2020).

Additionally, we identified FMRP expression in mature glial cells situated in the rat and chicken AG. In the peripheral auditory system, Schwann cells and satellite glial cells are the major glial cell types that wrap the processes and cell bodies of AG neurons, respectively. In particular, satellite glial cells are thought to play a role in maintaining the microenvironment

and facilitating communication between neuronal cell somata (Hanani, 2010). Drug-induced demyelination, i.e., deficiency of these glial cells, can lead to sensorineural hearing loss (El-Badry and McFadden, 2007; El-Badry et al., 2007; Locher et al., 2014). In this study, we identified cytoplasmic FMRP in satellite glial cells of both rodents and chickens as well as FMRP-containing envelops surrounding AG neurons in chickens. In the brain, astrocyte-specific loss of FMRP disrupts astrocytic mGluR5 signaling, alters neuronal dendritic and synaptic development, and contributes to cortical hyperexcitability (Jacobs et al., 2010, 2012; Men et al., 2020; Jin et al., 2021). Determining the significance of FMRP expression in satellite glial cells requires functional analyses.

CONCLUSION

The evolutionally conserved expression of FMRP in the vertebrate auditory periphery (hair cells and AG/SG neurons) suggests FMRP as an important player in cochlear development and function. Future investigations should be geared toward the identification of alterations in the cochlea following FMRP misexpression, particularly in AG/SG neurons and their projection to the brain (Wang et al., 2018). FMRP expression has also been identified in the retina and is regulated by visual experience (Frederikse et al., 2015; Guimarães-Souza et al., 2016), supporting an importance of peripheral FMRP across sensory modalities.

Acknowledgments

This study was supported by the National Institute of Health (R01MH126176 and R21DC17267) to Y.W, and grants to X.W: National Natural Science Foundation of China grant (No. 32000697), Science and Technology Program of Guangzhou (202102080139), Guangdong Natural Science Foundation (2019A1515110625, 2021A1515010619), The Fundamental Research Funds for the Central Universities (11620324), Research Grant of Key Laboratory of Regenerative Medicine, Ministry of Education, Jinan University (No. ZSYXM202107).

We thank Dr. Dongqing Cai (Jinan University) for providing the rat cochleae and Dr. Terra Bradley (Florida State University) for the careful editing of the manuscript. We thank the Medical experimental center of Jinan University.

Data Availability Statement

Data sharing is not applicable to this article as no new data were created or analyzed in this study.

Abbreviations

AG	auditory ganglion
BP	basilar papilla
FMRP	Fragile X mental retardation protein
FXS	Fragile X syndrome
IHC	inner hair cell
KO	knockout
OHC	outer hair cell

SHC	short hair cells
SG	spiral ganglion
SV	stria vascularis
THC	tall hair cells
Tuj1	neuron-specific class III beta-tubulin
WT	wildtype

References Cited

Arinami T, Sato M, Nakajima S, Kondo I. 1988. Auditory brain-stem responses in the fragile X syndrome. Am J Hum Genet 43:46–51. [PubMed: 3376943]

Bagni C, Tassone F, Neri G, Hagerman R. 2012. Fragile X syndrome: causes, diagnosis, mechanisms, and therapeutics. J Clin Invest 122:4314–4322. [PubMed: 23202739]

Beebe K, Wang Y, Kulesza R. 2014. Distribution of fragile X mental retardation protein in the human auditory brainstem. Neuroscience 273:79–91. [PubMed: 24838064]

Brackett DM, Qing F, Amieux PS, Sellers DL, Horner PJ, Morris DR. 2013. Fmr1 Transcript Isoforms: Association with Polyribosomes; Regional and Developmental Expression in Mouse Brain. PLOS ONE 8:e58296. [PubMed: 23505481]

Brown MR, Kronengold J, Gazula V-R, Chen Y, Strumbos JG, Sigworth FJ, Navaratnam D, Kaczmarek LK. 2010. Fragile X mental retardation protein controls gating of the sodium-activated potassium channel Slack. Nat Neurosci 13:819–821. [PubMed: 20512134]

Chervenak AP, Hakim IS, Barald KF. 2013. Spatiotemporal expression of Zic genes during vertebrate inner ear development. Dev Dyn 242:897–908. [PubMed: 23606270]

Connelly CJ, Ryugo DK, Muniak MA. 2017. The effect of progressive hearing loss on the morphology of endbulbs of Held and bushy cells. Hearing Research 343:14–33. [PubMed: 27473502]

Constantin L, Poulsen RE, Scholz LA, Favre-Bulle IA, Taylor MA, Sun B, Goodhill GJ, Vanwalleghem GC, Scott EK. 2020. Altered brain-wide auditory networks in a zebrafish model of fragile X syndrome. BMC Biol 18:125. [PubMed: 32938458]

Cook D, Sanchez-Carbente M del R, Lachance C, Radzioch D, Tremblay S, Khandjian EW, DesGroseillers L, Murai KK. 2011. Fragile X related protein 1 clusters with ribosomes and messenger RNAs at a subset of dendritic spines in the mouse hippocampus. PLoS ONE 6:e26120. [PubMed: 22022532]

Darnell JC, Van Driesche SJ, Zhang C, Hung KYS, Mele A, Fraser CE, Stone EF, Chen C, Fak JJ, Chi SW, Licatalosi DD, Richter JD, Darnell RB. 2011. FMRP Stalls Ribosomal Translocation on mRNAs Linked to Synaptic Function and Autism. Cell 146:247–261. [PubMed: 21784246]

Davis JK, Broadie K. 2017. Multifarious Functions of the Fragile X Mental Retardation Protein. Trends Genet 33:703–714. [PubMed: 28826631]

Deng P-Y, Rotman Z, Blundon JA, Cho Y, Cui J, Cavalli V, Zakharenko SS, Klyachko VA. 2013. FMRP regulates neurotransmitter release and synaptic information transmission by modulating action potential duration via BK channels. Neuron 77:696–711. [PubMed: 23439122]

Deng P-Y, Sojka D, Klyachko VA. 2011. Abnormal presynaptic short-term plasticity and information processing in a mouse model of fragile X syndrome. J Neurosci 31:10971–10982. [PubMed: 21795546]

Dury AY, El Fatimy R, Tremblay S, Rose TM, Côté J, De Koninck P, Khandjian EW. 2013. Nuclear Fragile X Mental Retardation Protein is localized to Cajal bodies. PLoS Genet 9:e1003890. [PubMed: 24204304]

Eichler EE, Richards S, Gibbs RA, Nelson DL. 1993. Fine structure of the human FMR1 gene. Human Molecular Genetics 2:1147–1153. [PubMed: 8401496]

El-Badry MM, Ding D, McFadden SL, Eddins AC. 2007. Physiological effects of auditory nerve myelinopathy in chinchillas. Eur J Neurosci 25:1437–1446. [PubMed: 17425569]

El-Badry MM, McFadden SL. 2007. Electrophysiological correlates of progressive sensorineural pathology in carboplatin-treated chinchillas. Brain Res 1134:122–130. [PubMed: 17198689]

El-Hassar L, Song L, Tan WJT, Large CH, Alvaro G, Santos-Sacchi J, Kaczmarek LK. 2019. Modulators of Kv3 Potassium Channels Rescue the Auditory Function of Fragile X Mice. J Neurosci 39:4797–4813. [PubMed: 30936239]

Fan Q, Zhang X, Wang Y, Wang X. 2022. Dissecting Cell-Autonomous Function of Fragile X Mental Retardation Protein in an Auditory Circuit by In Ovo Electroporation. JoVE (Journal of Visualized Experiments): e64187.

Ferri R 1989. Brain-stem auditory evoked potentials in the fragile X syndrome. Am J Hum Genet 45:977–979. [PubMed: 2589325]

Ferron L 2016. Fragile X mental retardation protein controls ion channel expression and activity. J Physiol 594:5861–5867. [PubMed: 26864773]

Fischer FP. 1994. General pattern and morphological specializations of the avian cochlea. Scanning Microsc 8:351–363; discussion 363–364. [PubMed: 7701304]

Frederikse PH, Nandanoor A, Kasinathan C. 2015. Fragile X Syndrome FMRP Co-localizes with Regulatory Targets PSD-95, GABA Receptors, CaMKIIα, and mGluR5 at Fiber Cell Membranes in the Eye Lens. Neurochem Res 40:2167–2176. [PubMed: 26298628]

Gholizadeh S, Halder SK, Hampson DR. 2015. Expression of fragile X mental retardation protein in neurons and glia of the developing and adult mouse brain. Brain Research 1596:22–30. [PubMed: 25446451]

Guimarães-Souza EM, Perche O, Morgans CW, Duvoisin RM, Calaza KC. 2016. Fragile X Mental Retardation Protein expression in the retina is regulated by light. Experimental Eye Research 146:72–82. [PubMed: 26719241]

Hagerman RJ, Berry-Kravis E, Hazlett HC, Bailey DB, Moine H, Kooy RF, Tassone F, Gantois I, Sonenberg N, Mandel JL, Hagerman PJ. 2017. Fragile X syndrome. Nat Rev Dis Primers 3:17065. [PubMed: 28960184]

Hamburger V, Hamilton HL. 1951. A series of normal stages in the development of the chick embryo. J Morphol 88:49–92. [PubMed: 24539719]

Hanani M 2010. Satellite glial cells in sympathetic and parasympathetic ganglia: In search of function. Brain Research Reviews 64:304–327. [PubMed: 20441777]

Heffner RS, Koay G, Heffner HE. 2001. Audiograms of five species of rodents: implications for the evolution of hearing and the perception of pitch. Hearing Research 157:138–152. [PubMed: 11470193]

Hill EM, Koay G, Heffner RS, Heffner HE. 2014. Audiogram of the chicken (Gallus gallus domesticus) from 2 Hz to 9 kHz. J Comp Physiol A Neuroethol Sens Neural Behav Physiol 200:863–870. [PubMed: 25092127]

Horn HF, Brownstein Z, Lenz DR, Shivatzki S, Dror AA, Dagan-Rosenfeld O, Friedman LM, Roux KJ, Kozlov S, Jeang K-T, Frydman M, Burke B, Stewart CL, Avraham KB. 2013. The LINC complex is essential for hearing. J Clin Invest 123:740–750. [PubMed: 23348741]

Huber KM, Gallagher SM, Warren ST, Bear MF. 2002. Altered synaptic plasticity in a mouse model of fragile X mental retardation. Proceedings of the National Academy of Sciences 99:7746–7750.

Jacobs S, Cheng C, Doering LC. 2012. Probing astrocyte function in fragile X syndrome. Results Probl Cell Differ 54:15–31. [PubMed: 22009345]

Jacobs S, Nathwani M, Doering LC. 2010. Fragile X astrocytes induce developmental delays in dendrite maturation and synaptic protein expression. BMC Neurosci 11:132. [PubMed: 20955577]

Jessen KR, Mirsky R. 2005. The origin and development of glial cells in peripheral nerves. Nat Rev Neurosci 6:671–682. [PubMed: 16136171]

Jin S-X, Higashimori H, Schin C, Tamashiro A, Men Y, Chiang MSR, Jarvis R, Cox D, Feig L, Yang Y. 2021. Astroglial FMRP modulates synaptic signaling and behavior phenotypes in FXS mouse model. Glia 69:594–608. [PubMed: 32970902]

Kazmierczak P, Sakaguchi H, Tokita J, Wilson-Kubalek EM, Milligan RA, Müller U, Kachar B. 2007. Cadherin 23 and protocadherin 15 interact to form tip-link filaments in sensory hair cells. Nature 449:87–91. [PubMed: 17805295]

Kelly JB, Masterton B. 1977. Auditory sensitivity of the albino rat. J Comp Physiol Psychol 91:930–936. [PubMed: 893752]

Kim H, Gibboni R, Kirkhart C, Bao S. 2013. Impaired critical period plasticity in primary auditory cortex of fragile X model mice. J Neurosci 33:15686–15692. [PubMed: 24089476]

Lai A, Valdez-Sinon AN, Bassell GJ. 2020. Regulation of RNA granules by FMRP and implications for neurological diseases. Traffic 21:454–462. [PubMed: 32374065]

Locher H, de Groot JCMJ, van Iperen L, Huisman MA, Frijns JHM, Chuva de Sousa Lopes SM. 2014. Distribution and development of peripheral glial cells in the human fetal cochlea. PLoS One 9: e88066. [PubMed: 24498246]

Lu R, Wang H, Liang Z, Ku L, O'donnell WT, Li W, Warren ST, Feng Y. 2004. The fragile X protein controls microtubule-associated protein 1B translation and microtubule stability in brain neuron development. Proc Natl Acad Sci USA 101:15201–15206. [PubMed: 15475576]

McCullagh EA, Rotschafer SE, Auerbach BD, Klug A, Kaczmarek LK, Cramer KS, Kulesza RJ, Razak KA, Lovelace JW, Lu Y, Koch U, Wang Y. 2020. Mechanisms underlying auditory processing deficits in Fragile X syndrome. FASEB J 34:3501–3518. [PubMed: 32039504]

Men Y, Ye L, Risgaard RD, Promes V, Zhao X, Paukert M, Yang Y. 2020. Astroglial FMRP deficiency cell-autonomously up-regulates miR-128 and disrupts developmental astroglial mGluR5 signaling. Proc Natl Acad Sci U S A 117:25092–25103. [PubMed: 32958647]

Pacey LKK, Doering LC. 2007. Developmental expression of FMRP in the astrocyte lineage: implications for fragile X syndrome. Glia 55:1601–1609. [PubMed: 17823967]

Pacey LKK, Xuan ICY, Guan S, Sussman D, Henkelman RM, Chen Y, Thomsen C, Hampson DR. 2013. Delayed myelination in a mouse model of fragile X syndrome. Human Molecular Genetics 22:3920–3930. [PubMed: 23740941]

Penagarikano O, Mulle JG, Warren ST. 2007. The Pathophysiology of Fragile X Syndrome. Annu Rev Genom Hum Genet 8:109–129.

Rais M, Binder DK, Razak KA, Ethell IM. 2018. Sensory Processing Phenotypes in Fragile X Syndrome. ASN Neuro 10:1759091418801092.

Roberts J, Hennon EA, Anderson K, Roush J, Gravel J, Skinner M, Misenheimer J, Reitz P. 2005. Auditory Brainstem Responses in Young Males With Fragile X Syndrome. J Speech Lang Hear Res 48:494–500. [PubMed: 15989407]

Rotschafer SE, Marshak S, Cramer KS. 2015. Deletion of Fmr1 Alters Function and Synaptic Inputs in the Auditory Brainstem. PLoS ONE 10: e0117266. [PubMed: 25679778]

Rotschafer SE, Razak KA. 2014. Auditory processing in fragile x syndrome. Front Cell Neurosci 8:19. [PubMed: 24550778]

Rubel EW, Fritzsch B. 2002. Auditory system development: primary auditory neurons and their targets. Annu Rev Neurosci 25:51–101. [PubMed: 12052904]

Ryan A 1976. Hearing sensitivity of the mongolian gerbil, Meriones unguiculatis. J Acoust Soc Am 59:1222. [PubMed: 956517]

Ryugo D 2015. Auditory neuroplasticity, hearing loss and cochlear implants. Cell Tissue Res 361:251–269. [PubMed: 25300646]

Santoro MR, Bray SM, Warren ST. 2012. Molecular mechanisms of fragile X syndrome: a twenty-year perspective. Annu Rev Pathol 7:219–245. [PubMed: 22017584]

Sinclair D, Oranje B, Razak KA, Siegel SJ, Schmid S. 2017. Sensory processing in autism spectrum disorders and Fragile X syndrome-From the clinic to animal models. Neurosci Biobehav Rev 76:235–253. [PubMed: 27235081]

Sotomayor M, Weihofen WA, Gaudet R, Corey DP. 2012. Structure of a force-conveying cadherin bond essential for inner-ear mechanotransduction. Nature 492:128–132. [PubMed: 23135401]

Tanaka K, Smith CA. 1978. Structure of the chicken's inner ear: SEM and TEM study. Am J Anat 153:251–271. [PubMed: 707316]

Verheij C, Bakker CE, de Graaff E, Keulemans J, Willemsen R, Verkerk AJ, Galjaard H, Reuser AJ, Hoogeveen AT, Oostra BA. 1993. Characterization and localization of the FMR-1 gene product associated with fragile X syndrome. Nature 363:722–724. [PubMed: 8515814]

Verkerk AJ, Pieretti M, Sutcliffe JS, Fu YH, Kuhl DP, Pizzuti A, Reiner O, Richards S, Victoria MF, Zhang FP. 1991. Identification of a gene (FMR-1) containing a CGG repeat coincident with a breakpoint cluster region exhibiting length variation in fragile X syndrome. Cell 65:905–914. [PubMed: 1710175]

Wang H, Ku L, Osterhout DJ, Li W, Ahmadian A, Liang Z, Feng Y. 2004. Developmentally-programmed FMRP expression in oligodendrocytes: a potential role of FMRP in regulating translation in oligodendroglia progenitors. Hum Mol Genet 13:79–89. [PubMed: 14613971]

Wang X, Kohl A, Yu X, Zorio DAR, Klar A, Sela-Donenfeld D, Wang Y. 2020. Temporal-specific roles of fragile X mental retardation protein in the development of the hindbrain auditory circuit. Development [Internet] 147. Available from: https://dev-biologists-org.proxy.lib.fsu.edu/content/147/21/dev188797

Wang X, Zorio DAR, Schecterson L, Lu Y, Wang Y. 2018. Postsynaptic FMRP Regulates Synaptogenesis In Vivo in the Developing Cochlear Nucleus. J Neurosci 38:6445–6460. [PubMed: 29950504]

Wang Y, Sakano H, Beebe K, Brown MR, de Laat R, Bothwell M, Kulesza RJ, Rubel EW. 2014. Intense and specialized dendritic localization of the fragile X mental retardation protein in binaural brainstem neurons: a comparative study in the alligator, chicken, gerbil, and human. J Comp Neurol 522:2107–2128. [PubMed: 24318628]

Yu X, Wang X, Sakano H, Zorio DAR, Wang Y. 2021. Dynamics of the fragile X mental retardation protein correlates with cellular and synaptic properties in primary auditory neurons following afferent deprivation. J Comp Neurol 529:481–500. [PubMed: 32449186]

Zhan X, Asmara H, Cheng N, Sahu G, Sanchez E, Zhang F-X, Zamponi GW, Rho JM, Turner RW. 2020. FMRP(1–297)-tat restores ion channel and synaptic function in a model of Fragile X syndrome. Nat Commun 11:2755. [PubMed: 32488011]

Zheng W, Holt JR. 2021. The Mechanosensory Transduction Machinery in Inner Ear Hair Cells. Annu Rev Biophys 50:31–51. [PubMed: 33285080]

Zorio DAR, Jackson CM, Liu Y, Rubel EW, Wang Y. 2017. Cellular distribution of the fragile X mental retardation protein in the mouse brain. J Comp Neurol 525:818–849. [PubMed: 27539535]

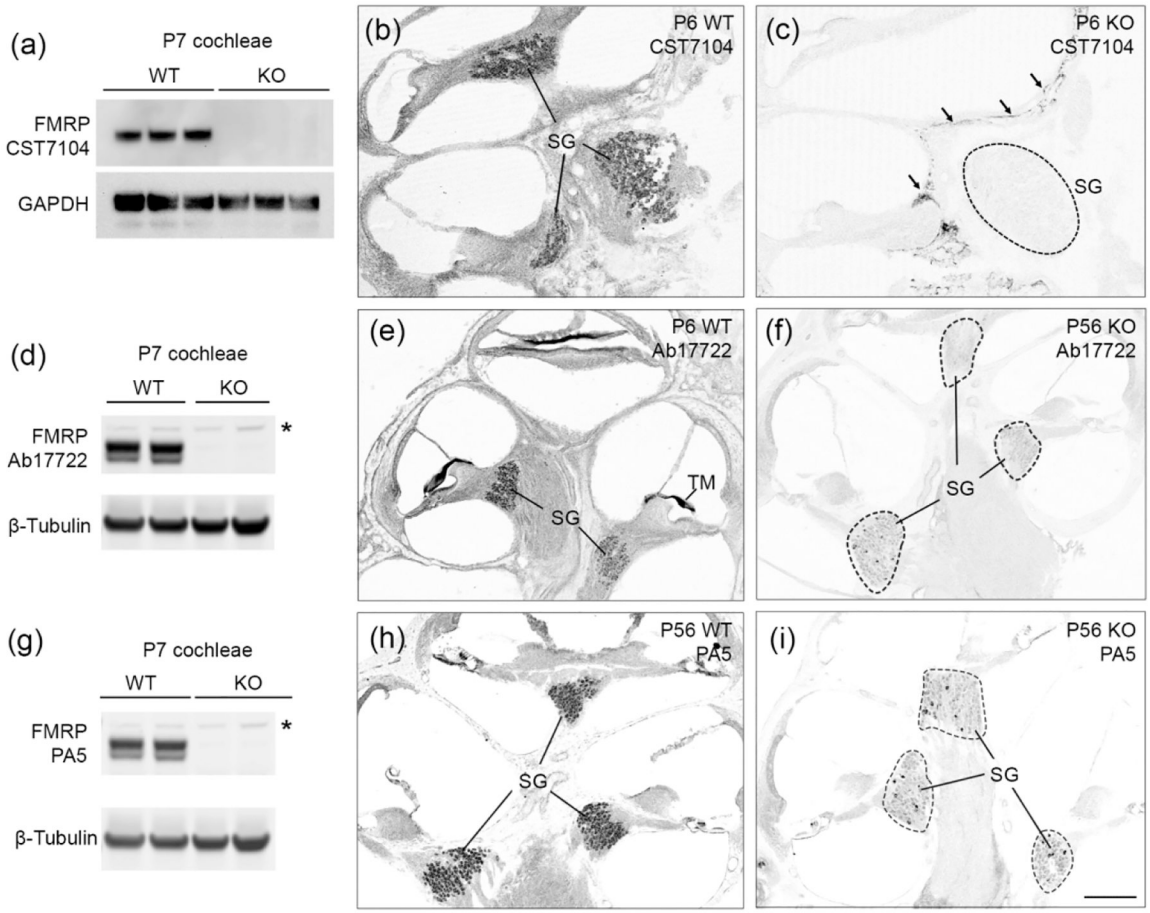

Figure 1.

Specificity characterization of anti-FMRP antibodies (CST7104, Ab17722, and PA5) in the mouse cochlea. (a) Western blot of CST7104 on cochlea samples collected from wildtype (WT) and *Fmr1* knockout (KO) mice. (b–c) Immunostaining of CST7104 on WT (b) and *Fmr1* KO (c) midmodiolar cross sections. Arrows in (c) point to nonspecific staining along the edge of the modiolous in the *Fmr1* KO. (d) Western blot of Ab17722 on cochlea samples collected from WT and *Fmr1* KO mice. The asterisk indicates a nonspecific band that was present in both genotypes. (e–f) Immunostaining of Ab17722 on WT (e) and *Fmr1* KO (f) cochlea sections. (g) Western blot of PA5 on cochlea samples collected from WT and *Fmr1* KO mice. The asterisk indicates a nonspecific band that was present in both genotypes. (h–i) Immunostaining of PA5 on WT (h) and *Fmr1* KO (i) cochlea sections. For western blot, each lane was an individual animal. Thirty micrograms of protein were loaded to each lane, with GAPDH or β-tubulin as the loading control. For immunocytochemistry, WT and KO sections were stained and imaged using the same parameters for comparison. Dashed circles outline the SG in the *Fmr1* KO. SG, spiral ganglion; TM, tectorial membrane. Scale bar in i = 200 μm, applies to b, c, e, f, h, i.

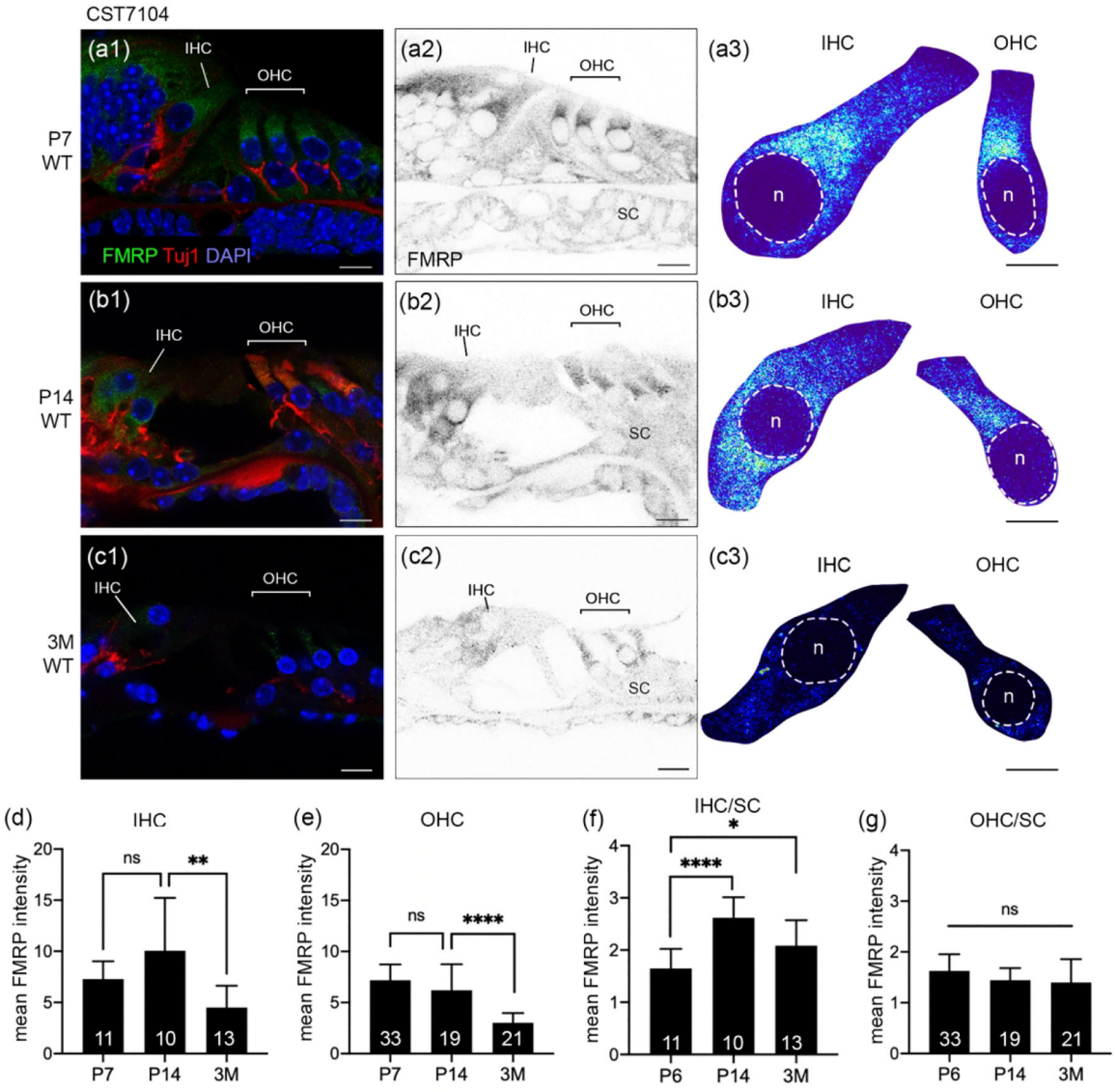

Figure 2.

FMRP_CST7104 immunostaining in the mouse organ of Corti during development. (a–c) CST7104 immunoreactivity on midmodiolar sections of WT mice at P7 (a1–a2), P14 (b1–b2), and 3 months (3M; c1–c2). Sections were also stained for Tuj1 immunoreactivity and DAPI counterstain. a3, b3, and c3 are heat maps of FMRP intensity in inner hair cells (IHCs) and outer hair cells (OHCs). Warm and cold colors represent high and low levels of FMRP intensity, respectively. For each age, the same color scale was applied to IHCs and OHCs. The nuclei of hair cells are outlined with dashed circles and labeled with "n". (d) Mean intensity of FMRP_CST7104 of IHCs. The number of hair cells measured at each age is indicated in the corresponding bar. Data were analyzed using one-way ANOVA followed by Tukey's multiple comparisons: F (2,25) = 5.915; $p = 0.0079$. (e) Mean intensity of FMRP_CST7104 of OHCs. One-way ANOVA: F (2,64) = 28.16; $p < 0.0001$. (f) Normalized FMRP_CST7104 intensity of the IHCs to that of supporting cells (SCs) on the same sections. One-way ANOVA: F (2,30) = 12.65; $p = 0.0001$. (g) Normalized FMRP_CST7104

intensity of the OHCs to that of SCs on the same sections. One-way ANOVA: F (2,70) = 3.261; $p = 0.0443$. *$p<0.05$; ****$p<0.0001$; ns, no significance. Scale bars = 10 μm in a1, a2, b1, b2, c1, c2; 5 μm in a3, b3, c3.

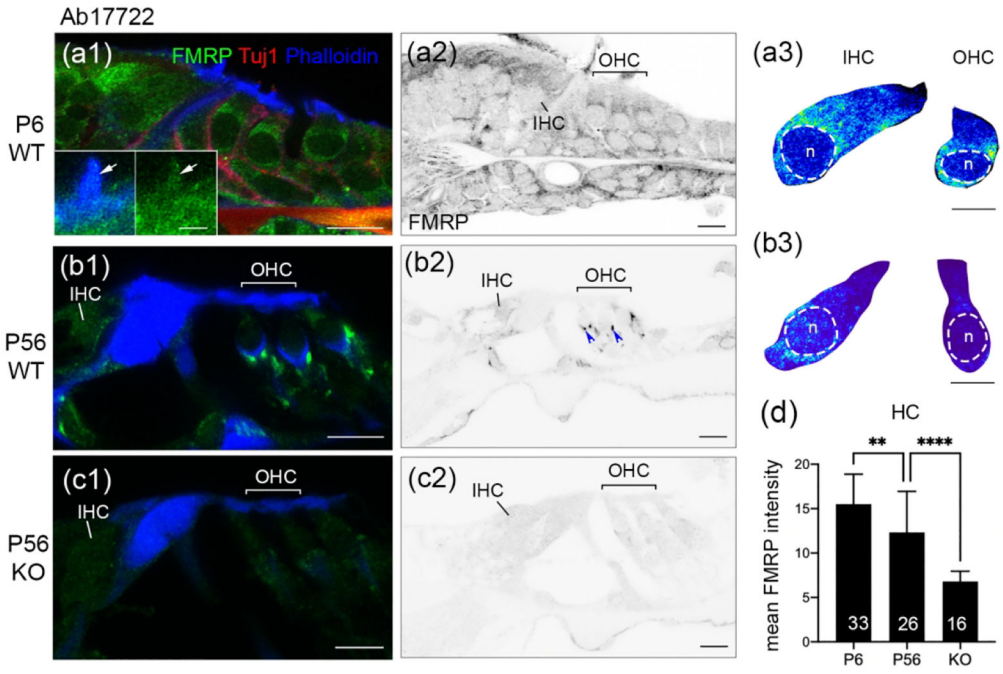

Figure 3.

FMRP_Ab17722 immunostaining in the mouse organ of Corti during development. (a–c) Ab17722 immunoreactivity on midmodiolar sections from WT P6 (a1–a2), WT P56 (b1–b2), and *Fmr1* KO P56 (c1–c2) mice. Sections were double stained for Tuj1 immunoreactivity and Phalloidin counterstain, a marker for hair bundles. Insets in a1 are magnifications of a hair cell bundle (white arrow). a3 and b3 are heat maps of FMRP intensity in inner hair cells (IHCs) and outer hair cells (OHCs) at P6 and P56, respectively. Warmer colors represent higher intensities of FMRP immunoreactivity than colder colors. At each age, the same color scale was applied to IHCs and OHCs. The nuclei of hair cells are outlined with dashed circles and labeled with “n”. (d) Mean intensity of FMRP_Ab17722 in hair cells. The number of hair cells measured is indicated in the corresponding bar. Data were analyzed by one-way ANOVA followed by Tukey’s multiple comparisons: $F(2,72) = 32.11$; $p < 0.0001$. **$p<0.01$; ****$p<0.0001$. Scale bars = 10 μm in a1, a2, b1, b2, c1, c2; 2 μm in inset of a1; 5 μm in a3, b3.

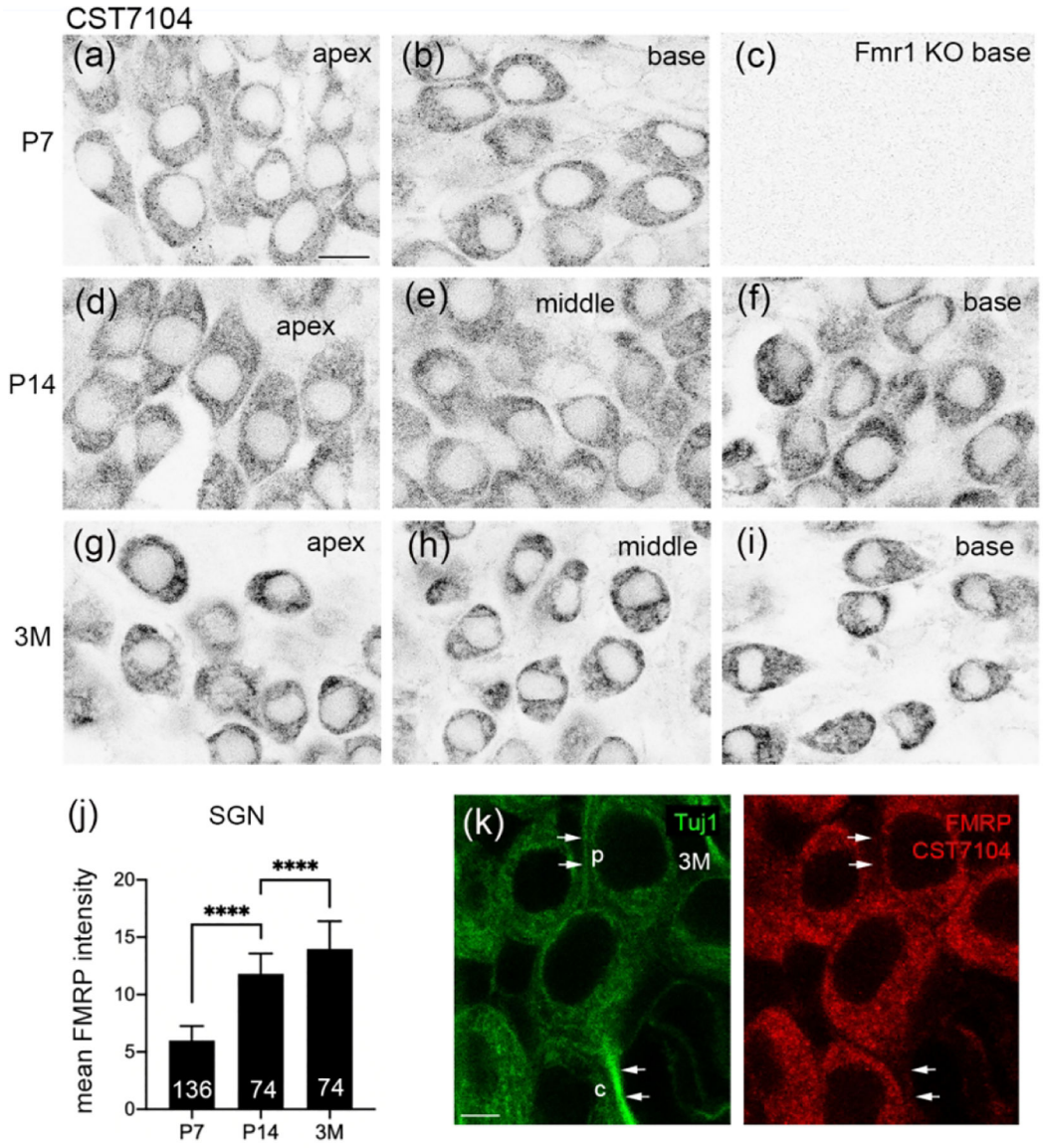

Figure 4.

FMRP_ CST7104 immunostaining in the mouse spiral ganglion (SG) during development. (a–c) CST7104 immunoreactivity at P7 in the apical (a) and basal (b) portions of the WT mouse and the basal portion of the *Fmr1* KO mouse (c). (d–f) CST7104 immunoreactivity at P14 in the apical (d), middle (e), and basal (f) portions of the WT mouse. (g–i) CST7104 immunoreactivity at 3 months in the apical (d), middle (e), and basal (f) portions of the WT mouse. (j) Mean intensity of FMRP_CST7104 in the SG neurons. The number of neurons measured in each group is indicated in the corresponding bar. Data were analyzed by one-way ANOVA followed by Tukey's multiple comparisons: F (2, 281) = 1155; $p<0.0001$. (k) FMRP immunostaining in the processes of SG neurons. Single focal plane of confocal image of double immunostaining of FMRP-CST7104 and Tuj1 in the SG of a 3-month-old WT mouse. Arrows point to the peripheral (p) and central (c) processes of a SG neuron. Scale bars = 10 μm in a, applies to a–I; 5 μm in k.

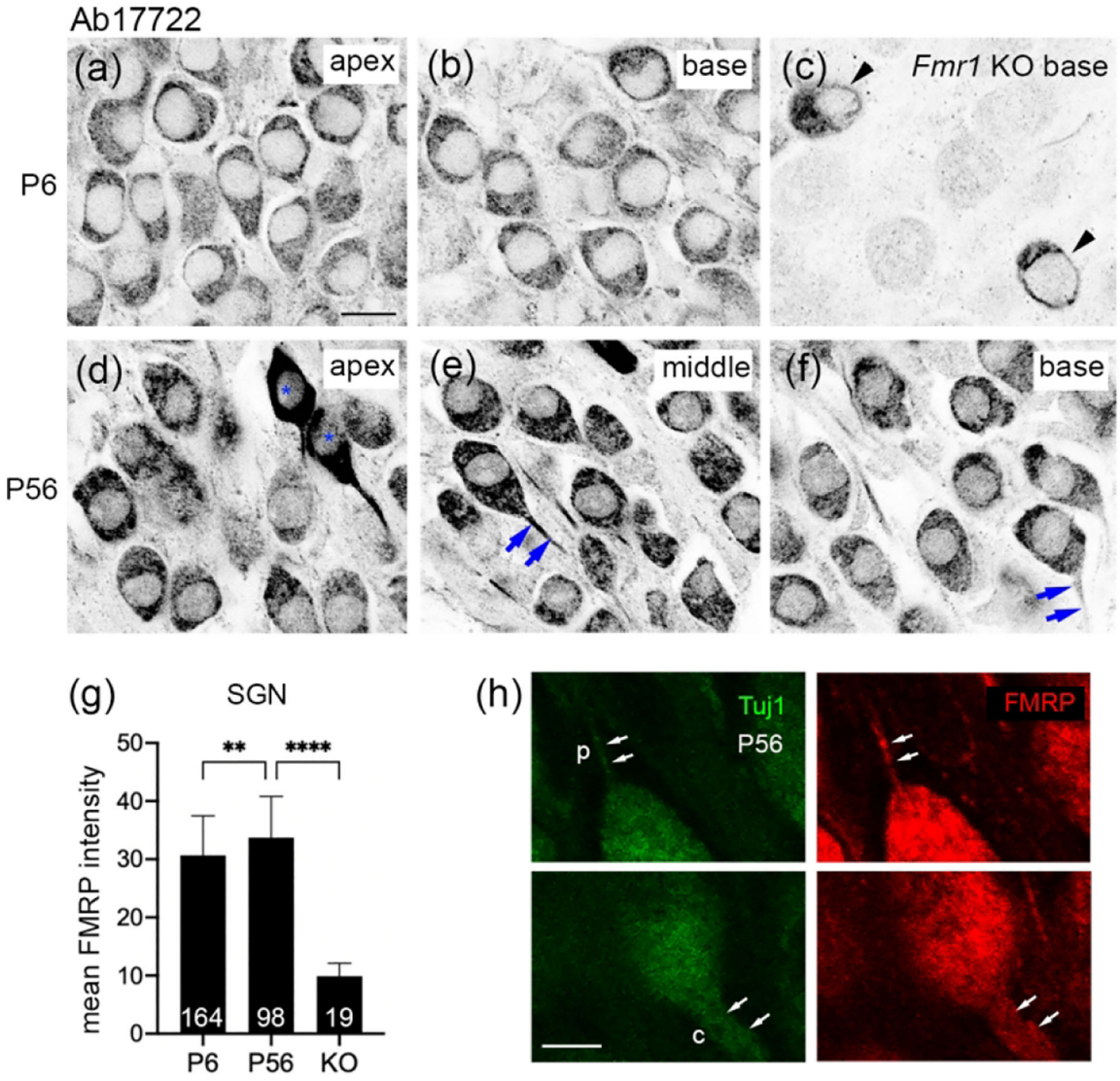

Figure 5.

FMRP_ Ab17722 immunostaining in the mouse spiral ganglion (SG) during development. (a–c) Ab17722 immunoreactivity at P6 in the apical (a) and basal (b) portions of the WT mouse and the basal portion of the *Fmr1* KO mouse (c). Arrowheads point to two neurons showing nonspecific staining. (d–f) Ab17722 immunoreactivity at P56 in the apical (d), middle (e), and basal (f) portions of the WT mouse. Asterisks label two neurons with intense Ab17722 staining in (d). Arrows point to Ab17722-labeled central axons. (g) Mean intensity of FMRP_Ab17722 in the SG neurons. The number of neurons measured in each group is indicated in the corresponding bar. Data were analyzed by one-way ANOVA followed by Tukey's multiple comparisons: F (2, 278) = 101.5; $p < 0.0001$. **$p<0.01$; ****$p<0.0001$. (h) FMRP immunostaining in the processes of SG neurons. Single focal plane of confocal image of double immunostaining of FMRP-Ab17722 and Tuj1 in the SG of a P56 WT mouse. Arrows point to the peripheral (p) and central (c) processes of a SG neuron. Scale bars = 10 μm in a, applies to a–f; 5 μm in h.

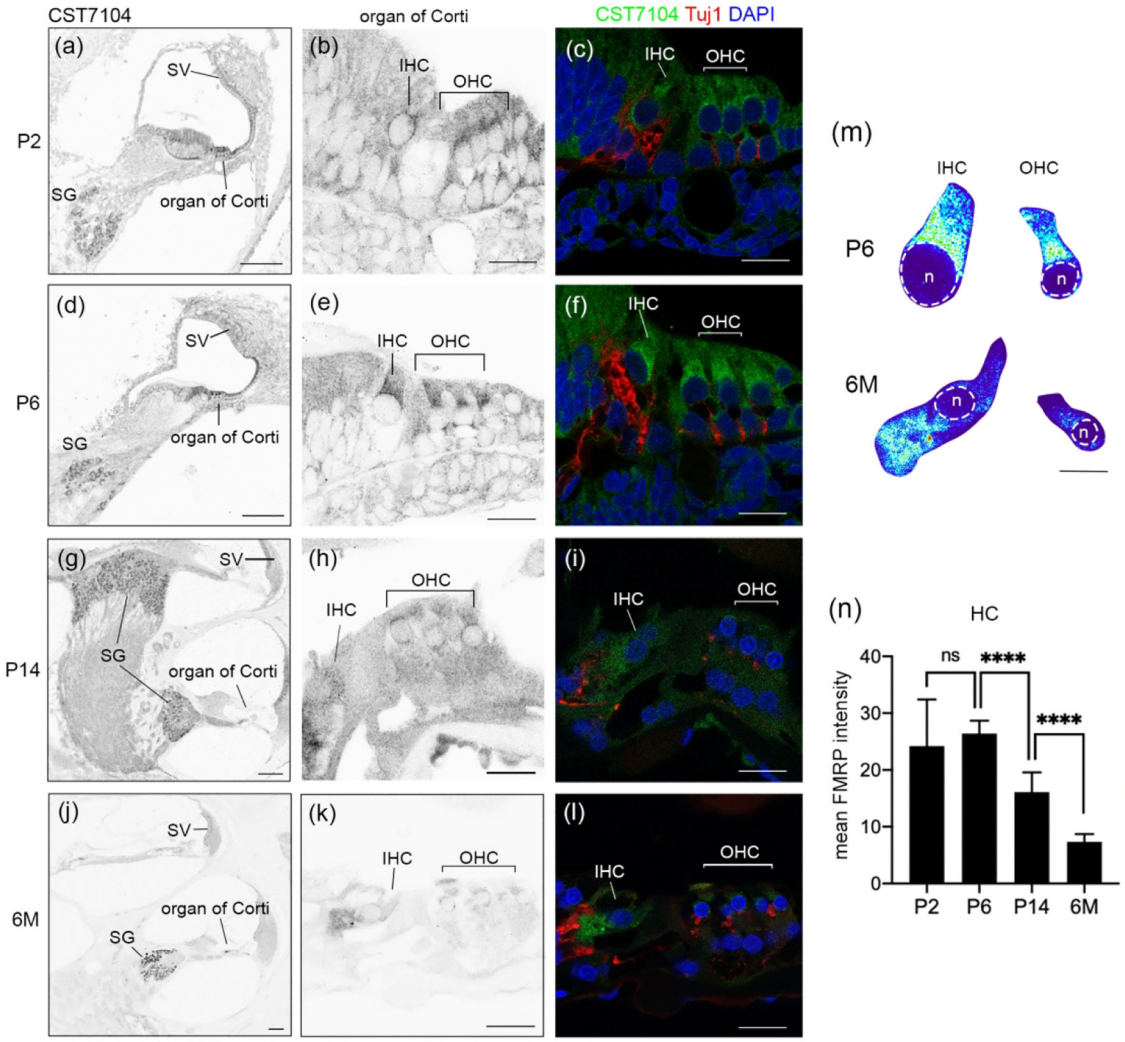

Figure 6.

FMRP in the rat cochlea during development. (a–l) FMRP-CST7104 immunoreactivity on the cochlear cross section at P2 (a–c), P6 (d–f), P14 (g–i), and 6 months (j–l). The left column (a, d, g, j) contains low-magnification images of the FMRP channel. The middle column (b, e, h, k) contains high-magnification images of the FMRP channel in the organ of Corti. The right column (c, f, I, l) contains the triple labeling of FMRP (green), Tuj1 (red), and DAPI (blue). (m) Heatmaps of FMRP intensity in inner hair cells (IHCs) and outer hair cells (OHCs) at P6 (upper) and 6M (lower), respectively. Warmer colors represent higher intensities of FMRP immunoreactivity than colder colors. At each age, the same color scale was applied to IHCs and OHCs. The nuclei of hair cells are outlined with dashed circles and labeled with “n”. (n) Mean intensity of FMRP_CST7104 in the hair cells. The number of hair cells measured in each group is indicated in the corresponding bar. Data were analyzed by one-way ANOVA followed by Tukey’s multiple comparisons: $F(3, 67) = 51.37$; $p < 0.0001$. ****$p<0.0001$; ns, no significance. Scale bars = 100 μm in the left column (a, d, g, j); 20 μm in the middle and right columns (b–c, e–f, h–I, k–l); and 10 μm in m.

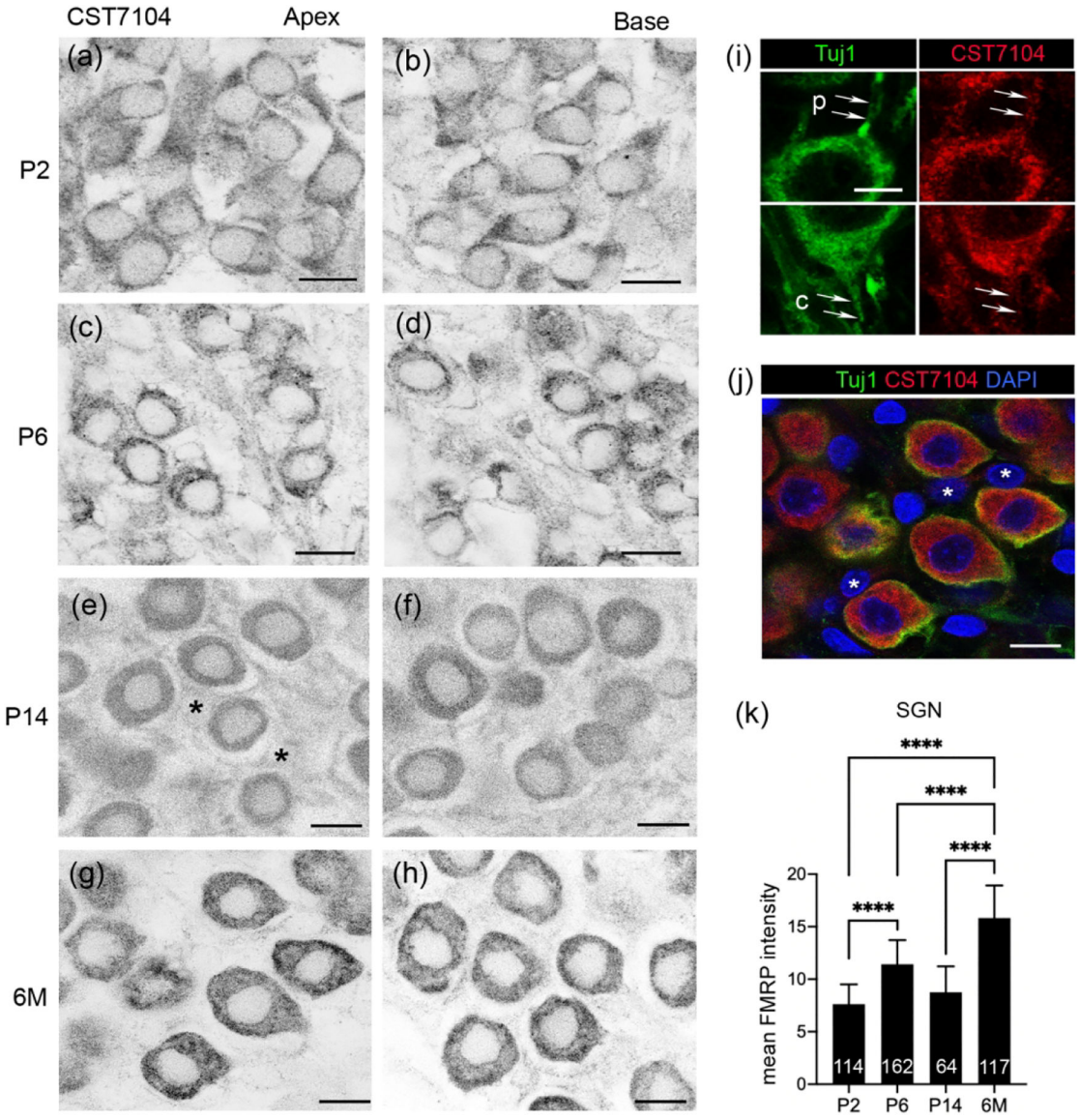

Figure 7.

FMRP_CST7104 immunostaining in the rat spiral ganglion (SG) during development. (a–h) CST7104 immunoreactivity at P2 (a–b), P6 (c–d), P14 (e–f), and 6 months (g–h). The left (a, c, e, g) and right (b, d, f, h) columns were taken from the apex and base of the SG, respectively. Asterisks in (e) indicate the nuclei of satellite glial cells. (i–j) Confocal images of double immunostaining of CST7104 and Tuj1 in the SG of a 6-month-old rat. Arrows point to the peripheral (p) and central (c) processes of a SG neuron. (j) Triple staining for FMRP and Tuj1 immunoreactivities as well as DAPI counterstain. The same region as in (g). White asterisks indicate the nuclei of satellite glial cells. (k) Mean intensity of FMRP_CST7104 in rat SG neurons. The number of neurons measured at each age is indicated in the corresponding bar. Data were analyzed by one-way ANOVA followed by Tukey's multiple comparisons: F (3, 453) = 251.5; $p < 0.0001$. ****$p<0.0001$. Scale bars = 10 μm in a–h, j; 5 μm in i.

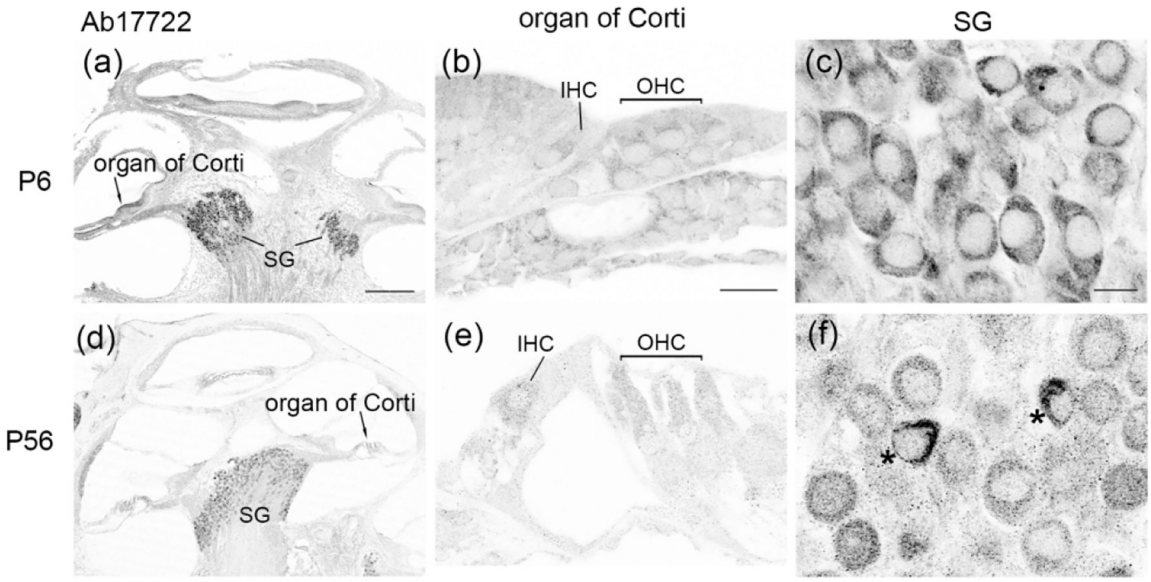

Figure 8.

FMRP_Ab17722 immunostaining in the gerbil cochlea during development. (a–c) were taken from a P6 gerbil. (d–f) were taken from a P56 gerbil. (a) and (d) are low-magnification images of the cochlea. (b) and (e) are high-magnification images of the organ of Corti. (c) and (f) were taken from the spiral ganglion (SG). Asterisks in (f) indicate two intensely stained SG neurons. Scale bars = 200 μm in a, applies to a, d; 20 μm in b, applies to b, e; 10 μm in c, applies to c, f.

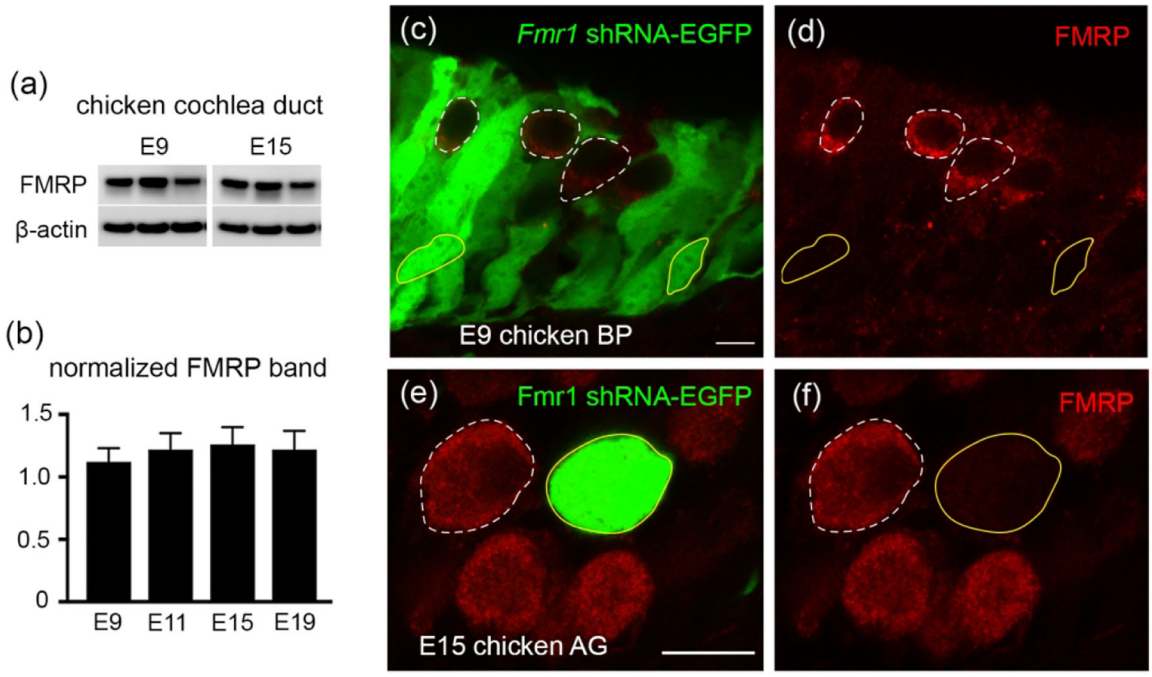

Figure 9.

Antibody characterization for FMRP_PA8263 in the chicken inner ear. (a) Western blot of FMRP on cochlea samples collected from E9 and E15 chicken embryos. (b) Bar chart of FMRP band intensity that was normalized to β-actin and plotted with age (one-way ANOVA: F (3,9) = 0.6702; $p = 0.5914$). (c–d) FMRP immunostaining (red) on the E9 basilar papilla (BP) transfected with *Fmr1* shRNA-EGFP (green). (e–f) FMRP immunostaining (red) on the E15 auditory ganglion (AG) transfected with *Fmr1* shRNA-EGFP (green). Yellow solid and white dashed circles are examples of transfected (EGFP positive) and non-transfected (EGFP negative) cells or neurons, respectively. Scale bars = 10 μm in c, applies to c–d; 10 μm in e, applies to e–f.

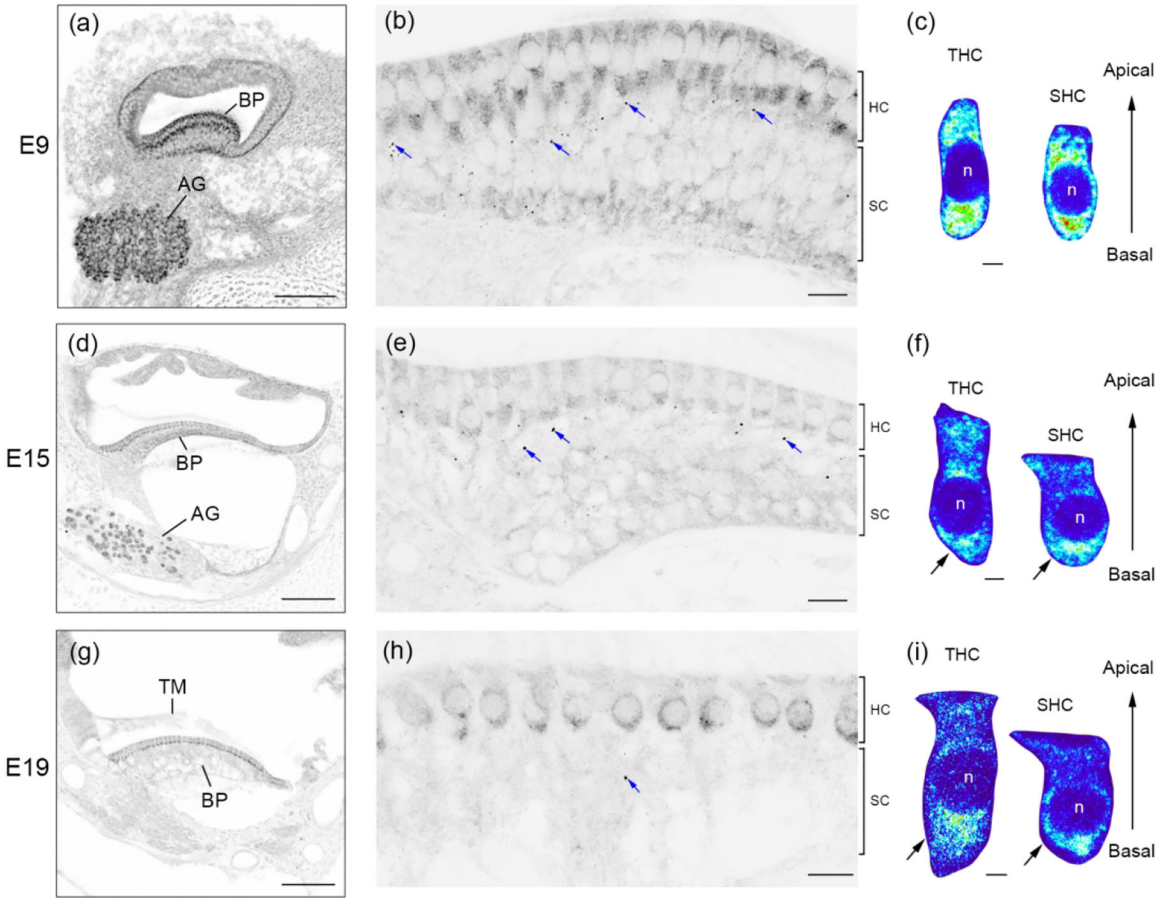

Figure 10.

FMRP_PA8263 immunostaining in the chicken basilar papilla (BP) during development. Images were taken at E9 (a–c), E15 (d–f), and E19 (g–i). The left column (a, d, g) contains low-magnification images of the cochlea cross section. The middle column (b, e, h) contains high-magnification images of the BP. Blue arrows point to darkly labeled FMRP puncta within the supporting cell (SC) layers. Additional images of these puncta are illustrated in Figure 16. The right column (c, f, i) contains heat maps of FMRP intensity in tall hair cells (THCs) and short hair cells (SHCs). Warm and cold colors represent high and low levels of FMRP intensity, respectively. Note that the color scale is the same for THCs and SHCs of the same age. The nuclei of hair cells are labeled with “n”. Scale bars = 100 μm in a, d, g; 10 μm in b, e, h; 2 μm in c, f, i.

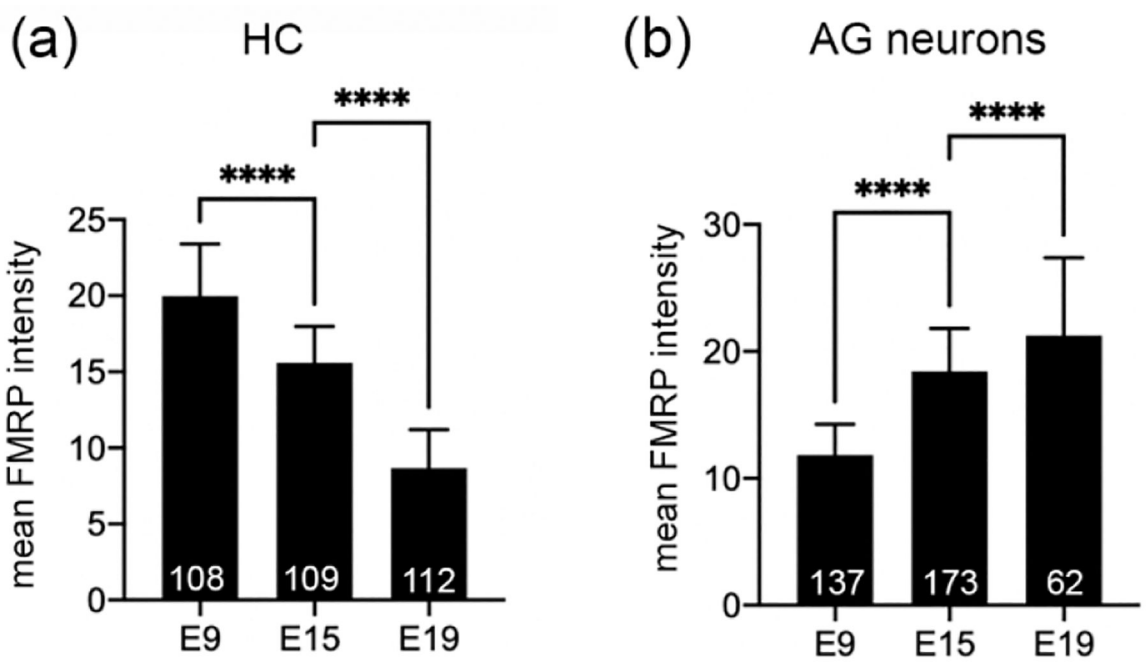

Figure 11.

Quantification of FMRP_PA8263 immunoreactivity in the chicken cochlear duct. The mean intensity of cytoplasmic FMRP immunoreactivity was measured from individual cells. The number of cells or neurons measured at each age is indicated in the corresponding bar. Data were analyzed by one-way ANOVA followed by Tukey's multiple comparisons. (a) FMRP intensity in hair cells: F (2, 326) = 451.1; $p < 0.0001$. (b) FMRP intensity in auditory ganglion (AG) neurons: F (2, 369) = 183.7; $p < 0.0001$. ****$p<0.0001$.

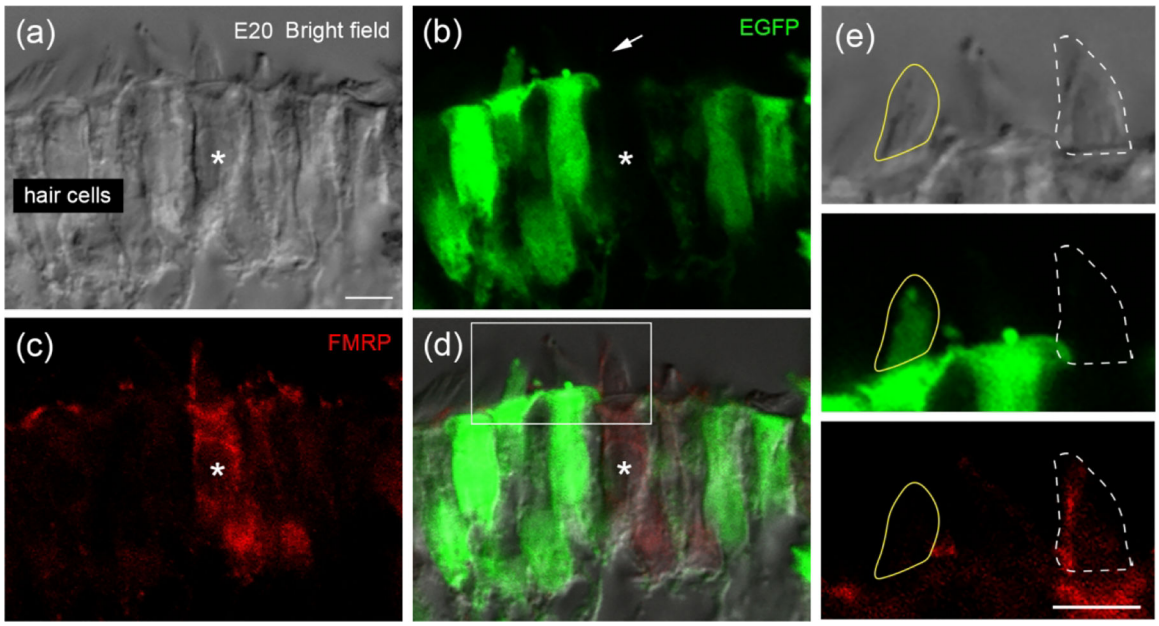

Figure 12.

FMRP localization in hair bundles of chicken hair cells. Chicken otocysts were transfected with *Fmr1* shRNA-EGFP at E2 via *in ovo* electroporation. FMRP immunostaining was performed at E20 on cochlea cross sections. (a) Hair cells under bright field with phase contrast. (b) *Fmr1* shRNA-EGFP (green). (c) FMRP_PA8263 immunoreactivity (red). (d) Merged image. Asterisks indicate a non-transfected hair cell showing FMRP-immunoreactive hair bundle (arrow). (e) Enlarged images of the box in d. Yellow circle outlines the hair bundle of a transfected hair cell (EGFP-positive) without detectable FMRP immunoreactivity. White dashed circle outlines the hair bundle of a non-transfected hair cell (EGFP-negative) showing distinct FMRP immunoreactivity. Scale bars = 5 μm in a, applies to a–d; 5 μm in e.

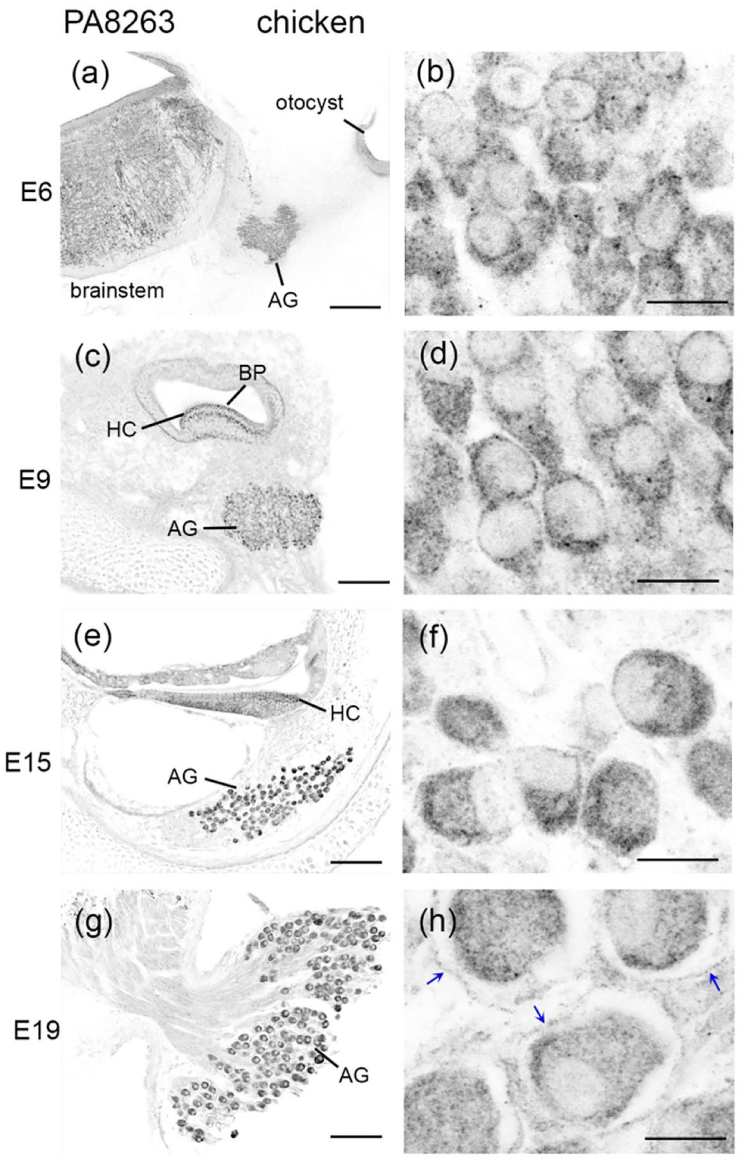

Figure 13.

FMRP_PA8263 immunostaining in the chicken auditory ganglion (AG) during development. Images were taken from E6 (a–b), E9 (c–d), E15 (e–f), and E19 (g–h) embryos. The left column (a, c, e, g) contains low-magnification images of cochlea cross sections; (a) shows head cross section at the otocyst level at E6. The right column (b, d, f, h) contains high-magnification images of the AG. Blue arrows in (h) indicate the FMRP envelope surrounding AG neurons. Scale bars = 200 μm in a; 100 μm in c, e; 50 μm in g; 10 μm in b, d, f, h.

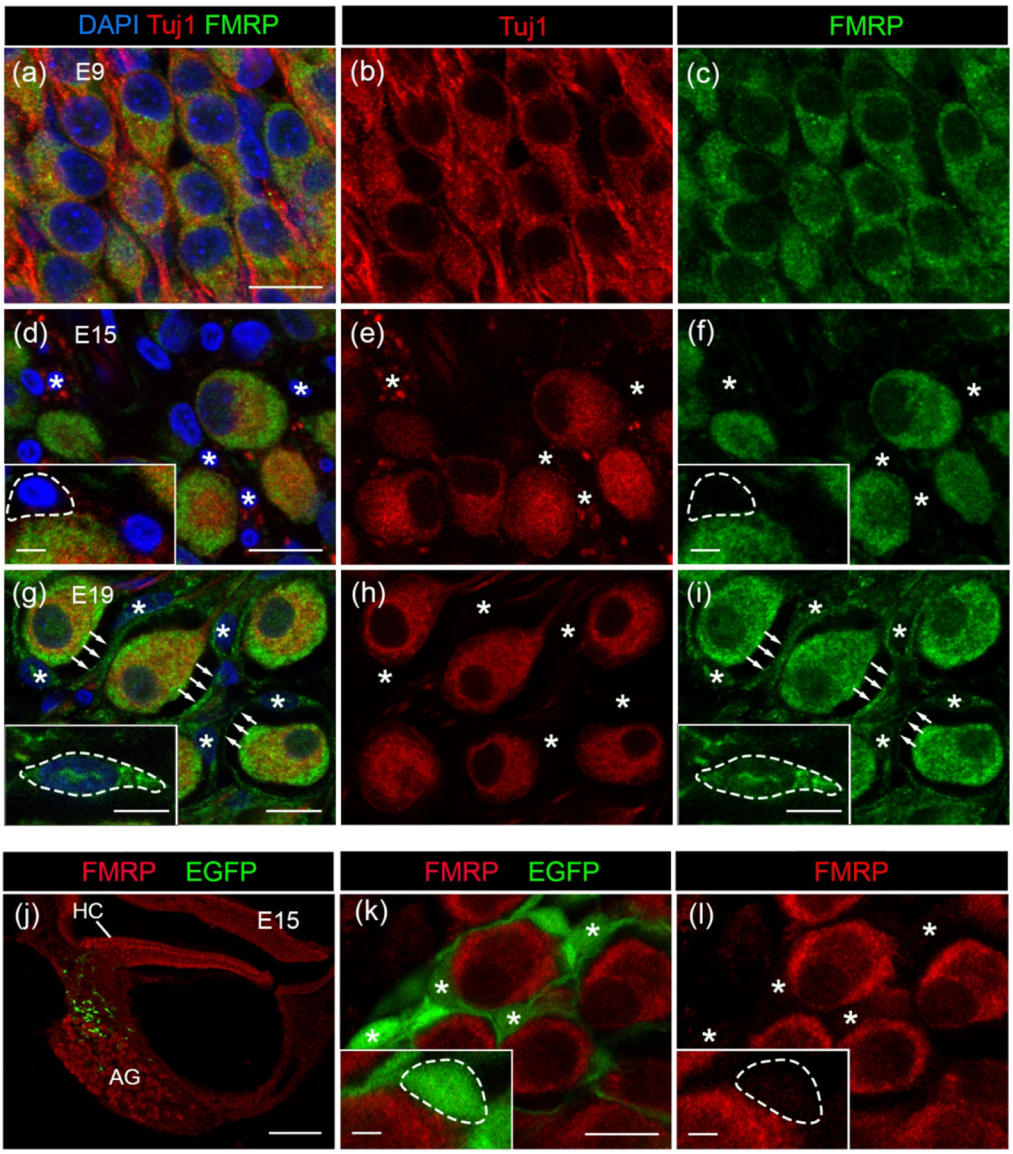

Figure 14.

FMRP_PA8263 immunostaining in the chicken satellite glial cells during development. (a–i) FMRP (green) and Tuj1 (red) double immunostaining on cochlea cross sections counterstained with DAPI (blue) at E9 (a–c), E15 (d–f), and E19 (g–i). Asterisks indicate the location of glial cell bodies. Arrows point along the FMRP-immunoreactive envelops surrounding AG neurons. Insets in d, f, g, and I show enlarged glial cell bodies with dashed outline. (j–l) PA8263 immunoreactivity (red) on cochlea cross sections from a E15 chicken embryo that was transfected with EGFP (green) via *in ovo* electroporation of scrambled Fmr1 shRNA-EGFP constructs (Wang et al., 2018). (j) and (k–l) are low- and high-magnification images of AG, respectively. AG neurons are surrounded by EGFP-positive glial cells and their processes, which contained no or little FMRP. Asterisks indicate the cell bodies of transfected satellite glial cells. Insets in k and l show enlarged glial cell soma with dashed outline. Scale bars = 10 μm in a, applies to a–c; 10 μm in d, applies to d–f;

10 μm in g, applies to g–i; 10 μm in k, applies to k–l; 100 μm in j; 2 μm in insets of d, f, k, l; 5 μm in insets of g, i.

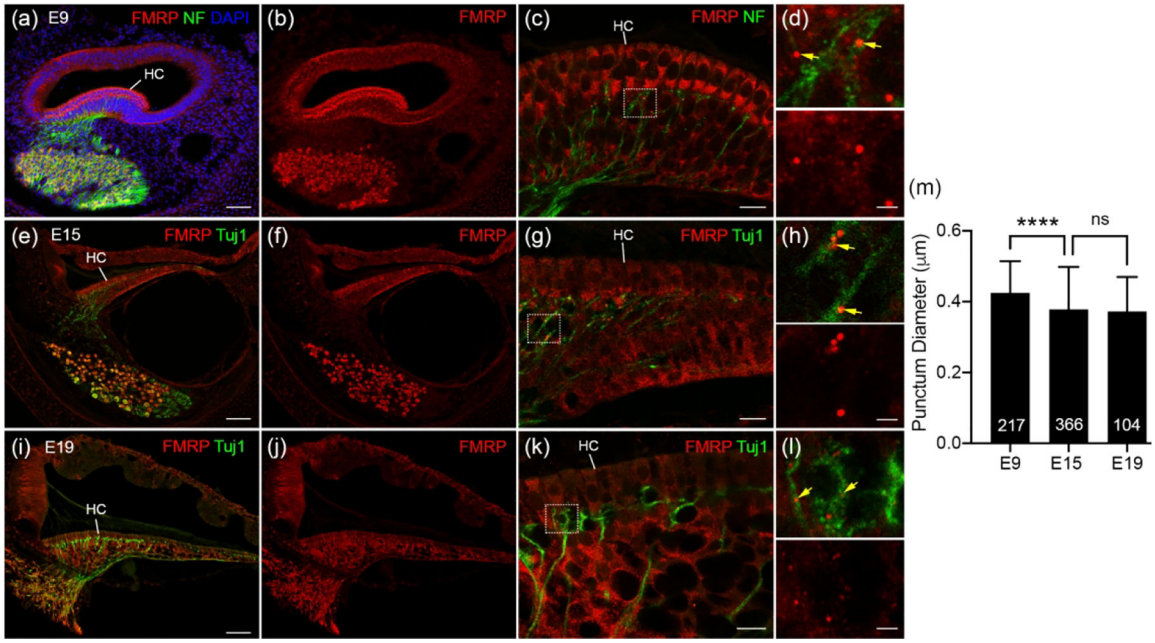

Figure 15.

FMRP_PA8263 immunostaining in the distal peripheral processes of chicken auditory ganglion (AG) during development. (a-b) Low-magnification images of FMRP (red) and Neurofilament (NF, green) double immunostaining on E9 cochlea cross section counterstained with DAPI (blue). (c) High-magnification of FMRP and NF immunostaining in the E9 BP. (d) Closer view of the box in c. Yellow arrows point to FMRP puncta located in NF-labeled processes. (e–f) Low-magnification of FMRP (red) and Tuj1 (green) double immunostaining in E15 cochlea. (g) High-magnification of FMRP and Tuj1 immunostaining in the E15 BP. (h) Closer view of the box in g. Yellow arrows point to FMRP puncta located in Tuj1-labeled processes. (i–j) Low-magnification images of FMRP (red) and Tuj1 (green) double staining in E19 cochlea. (k) High-magnification images of FMRP and Tuj1 immunostaining in the E19 BP. (l) Closer view of the box in k. Yellow arrows point to FMRP puncta located in Tuj1-labeled processes. (m) Quantification of FMRP punctum size. The punctum diameter is 0.42 ± 0.09 μm at E9, 0.38 ± 0.12 μm at E15, and 0.37± 0.10 μm at E19. One-way ANOVA was performed followed by Tukey's multiple comparisons: $F(2, 684) = 14.70$. ****$p<0.0001$; ns, not significant. Scale bars = 50 μm in a, applies to a–b; 50 μm in e, applies to e–f; 50 μm in i, applies to i–j; 10 μm in c, g, k; 2 μm in d, h, l.

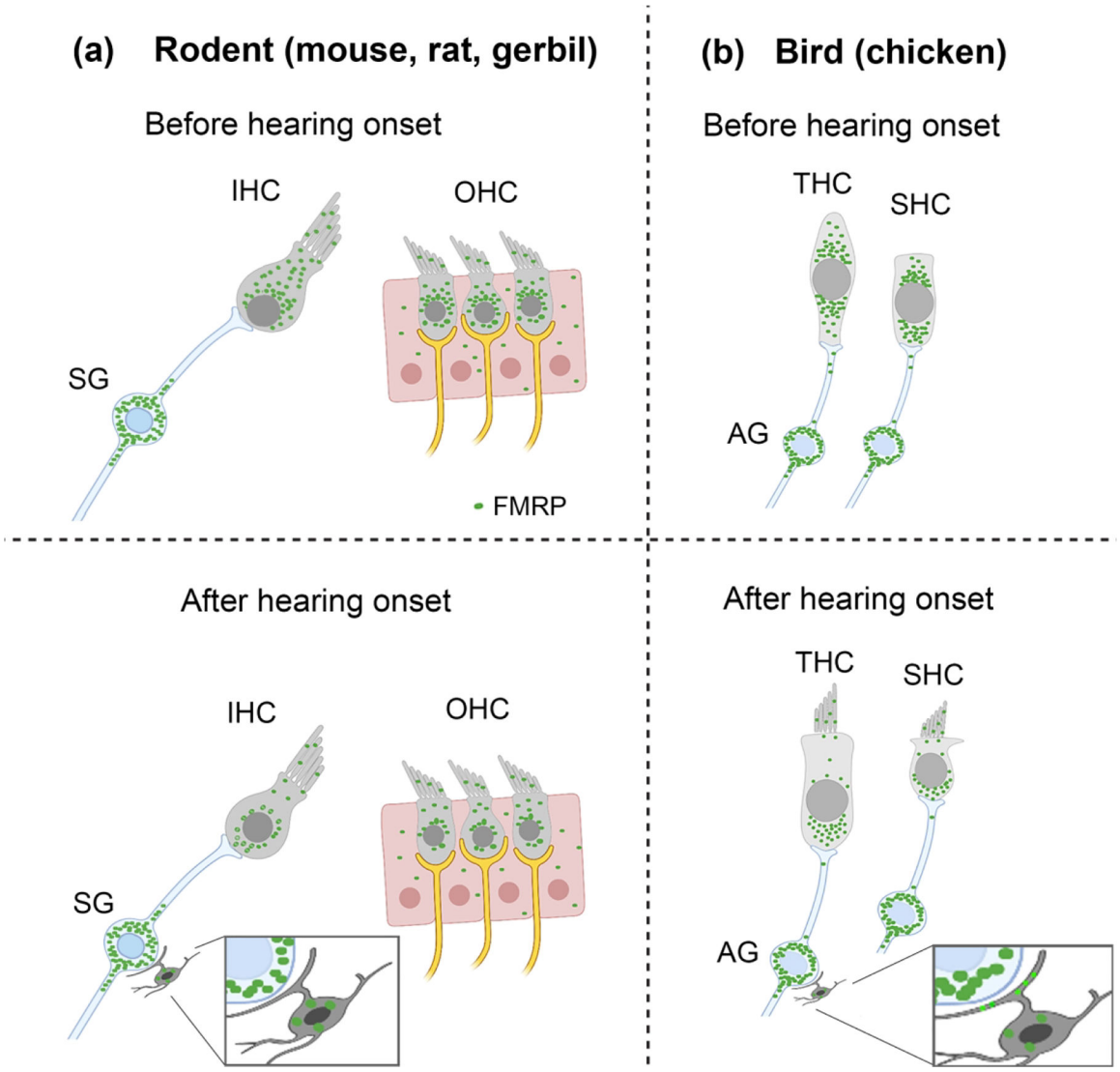

Figure 16.

Schematic drawings of FMRP profile in the cochlea. (a) FMRP expression pattern in the organ of Corti and spiral ganglion (SG) in rodents before and after hearing onset. (b) FMRP expression pattern in the chicken hair cells and auditory ganglion (AG). Green particles indicate the presence of FMRP immunoreactivity.

Table 1.

Primary antibodies used for immunocytochemistry (ICC) and western blot (WB)

	Antigen	Host, mono- or polyclonal, working dilution	RRID citation
CST7104	residues surrounding Gly552 of human FMRP protein	Rabbit, monoclonal, 1:100 (ICC); 1:1000 (WB)	Cell Signaling Technology Cat# 7104, RRID: AB_10950502
Ab17722	within human FMRP aa 550 to the C-terminus	Rabbit, polyclonal, 1:1000 (ICC & WB)	Abcam Cat# ab17722, RRID: AB_2278530
PA5	within human FMRP aa 550 to the C-terminus	Rabbit, polyclonal, 1:1000 (ICC & WB)	Thermo Fisher Scientific Cat# PA5–34584, RRID: AB_2551936
PA8263	KGNDEQSRTDNRQRNSRD A, near the C-terminus of the chicken full length FMRP protein	Rabbit, polyclonal, 1:1000 (ICC & WB)	Y. Wang, Florida State University Cat# FMRP_8263, RRID: AB_2861242
Tuj1	Synthetic peptide corresponding to rat beta III tubulin aa 400–500	Mouse, monoclonal, 1:1000 (ICC)	Abcam Cat# ab78078, RRID: AB_2256751